Book Chapter

The Lateral Superior Olive in the Mouse: Two Systems of Projecting Neurons

Isabella R Williams[1,2]*, Anastasia Filimontseva[1], Catherine J Connelly[1,2†] and David K Ryugo[1,2,3]

[1]Garvan Institute of Medical Research, Darlinghurst, NSW, Australia
[2]School of Medical Sciences, University of New South Wales, Kensington, NSW, Australia
[3]Department of Otolaryngology-Head, Neck and Skull Base Surgery, St. Vincent's Hospital, Darlinghurst, NSW, Australia

[†]Present address: Catherine J. Connelly, Department of Otolaryngology-Head and Neck Surgery, Johns Hopkins University School of Medicine, Baltimore, MD, United States

***Corresponding Author:** Isabella R Williams, Garvan Institute of Medical Research, Darlinghurst, NSW, Australia

Published **January 13, 2023**

This Book Chapter is a republication of an article published by Isabella R Williams, et al. at Frontiers in Neural Circuits in October 2022. (Williams IR, Filimontseva A, Connelly CJ and Ryugo DK (2022) The lateral superior olive in the mouse: Two systems of projecting neurons. Front. Neural Circuits 16:1038500. doi: 10.3389/fncir.2022.1038500)

How to cite this book chapter: Isabella R Williams, Anastasia Filimontseva, Catherine J Connelly, David K Ryugo. The Lateral Superior Olive in the Mouse: Two Systems of Projecting Neurons. In: Prime Archives in Neuroscience: 2nd Edition. Hyderabad, India: Vide Leaf. 2023.

Acknowledgements: The authors thank Giedre Milinkeviciute, Michael A. Muniak, Kirupa Suthakar, and Valentina Vanghi for their technical contributions. The authors also extend their thanks to the reviewers for their constructive criticism of this manuscript.

Conflicts of Interest: The authors declare that the research was conducted in the absence of any commercial or financial relationships that could be construed as a potential conflict of interest.

Author Contribution Statement: IRW, AF, and DKR designed the research; IRW, AF, and CJC conducted animal work and histological processing; IRW and AF analyzed the data under the supervision of DKR; IRW and DKR composed the first draft; figures were created by IRW, AF and DKR; all authors contributed to the final draft of the manuscript and verify the accuracy and integrity of the work; DKR secured funding for the project.

Data Availability Statement: The data that support this study can be requested from the corresponding author.

Funding Information: NHMRC Grant 1080652 to DKR; a bequest from Helen Morgan and gifts from Sue and Haydn Daw, Charlene and Graham Bradley, and Alan and Lynn Rydge for Hearing Research. CJC was recipient of a University International Postgraduate Award from the UNSW Australia. The donors had no role in the direction, analysis, or publication of this work.

Abstract

The lateral superior olive (LSO) is a key structure in the central auditory system of mammals that exerts efferent control on cochlear sensitivity and is involved in the processing of binaural level differences for sound localization. Understanding how the LSO contributes to these processes requires knowledge about the resident cells and their connections with other auditory structures. We used standard histological stains and retrograde tracer injections into the inferior colliculus (IC) and cochlea in order to characterize two basic groups of neurons: (1) Principal and periolivary (PO) neurons have projections to the inferior colliculus (IC) as part of the ascending auditory pathway; and (2) lateral olivocochlear (LOC) intrinsic and shell efferents have descending projections to the cochlea. Principal and intrinsic neurons are intermixed within the LSO, exhibit fusiform somata, and have disk-shaped dendritic arborizations. The principal neurons have bilateral, symmetric, and tonotopic projections to the IC. The intrinsic efferents have strictly ipsilateral projections, known to be tonotopic from previous publications. PO and shell neurons represent much smaller populations (<10% of principal and intrinsic neurons, respectively), have multipolar somata, reside outside the LSO, and have non-topographic, bilateral projections. PO and shell neurons appear to have widespread projections to their targets that imply a more diffuse modulatory function. The somata and dendrites of principal and intrinsic neurons form a laminar matrix within the LSO and share quantifiably similar alignment to the tonotopic axis. Their restricted projections emphasize the importance of frequency in binaural processing and efferent control for auditory perception. This study addressed and expanded on previous findings of cell types, circuit laterality, and projection tonotopy in the LSO of the mouse.

Keywords

Anatomy; Auditory; Isofrequency; Lateral Superior Olive; Olivocochlear Efferents; Topography; Tonotopy

Abbreviations

AChE- Acetylcholinesterase; AR- Antonia Red Dextran 4; AVCN- Anteroventral Cochlear Nucleus; C- Caudal; CF- Characteristic Frequency; ChAT- Choline Acetyltransferase; CN- Cochlear Nucleus; CNIC- Central Nucleus of the Inferior Colliculus; CTB- Cholera Toxin Subunit-B; CV- Cresyl Violet; D- Dorsal; DH- Dorsal Hilus; DAB-3,3'-diaminobenzene; FD- Fluorescein Dextran; FG- Fluorogold; IC- Inferior Colliculus; L- Lateral; LOC- Lateral Olivocochlear; LSO- Lateral Superior Olive; MNTB- Medial Nucleus of the Trapezoid Body; MOC- Medial Olivocochlear; NiDAB- Nickel Intensified DAB; OC- Olivocochlear; PO- Periolivary; SOC- Superior Olivary Complex

Introduction

The perception of auditory space is initiated by the complementary actions of multiple auditory brainstem nuclei. Anatomical and physiological data implicate the medial superior olive in the processing of interaural time differences, the lateral superior olive (LSO) and medial nucleus of the trapezoid body (MNTB) in decoding interaural level differences, and the dorsal cochlear nucleus (CN) for analysing spectral cues created by head and pinna reflections [1-8]. The LSO is part of the superior olivary complex (SOC), located at the base of the pontine-medullary junction and is one of the earliest structures to receive binaural inputs. Basic knowledge about LSO cell morphology and how they are synaptically connected represents an important first step to understanding the circuits for the localization and separation of sounds.

Auditory information that reaches the LSO originates directly from ipsilateral spherical bushy and planar multipolar cells of the anteroventral cochlear nucleus (AVCN; [9,10]) and indirectly from contralateral globular bushy cells of the AVCN by way of the MNTB [11-15]. The convergence of these two inputs, one excitatory and the other inhibitory, are matched in frequency tuning and temporal characteristics for analysis of interaural level differences, a primary cue for localizing high frequency

sounds [16]. The result of this binaural processing is sent along ascending pathways for further encoding of spatial location [17,18] and down descending pathways to modulate cochlear sensitivity in ways yet to be fully understood.

The LSO contains a heterogeneous population of neurons that have been categorized on the basis of somatic size, dendritic morphology, location [19-24], chemical markers [25,26], or projections [27-29]. These different neuron groups are presumably involved in separate aspects of processing and dispensing this information. The dominant LSO cell type is the principal neuron and they have ascending projections up the midbrain [20,21,27,28]. Other cell types have been described and vary with respect to species, staining technique, taxonomic criteria, and observer. Four cell types are proposed for the cat [21], four for the gerbil [22], three for the mouse [19], three for the human [30], and seven for the rat [23]. The main limitation to these taxonomic schemes is that they do not include circuit information and they are founded on observations collected from different species of widely different ages, crucial variables known to influence structure and function [31-35].

The other main type of LSO neuron in the mouse is the intrinsic neuron, which comprises the group of lateral olivocochlear (LOC) efferents, whose axonal projections terminate under inner hair cells of the cochlea primarily against the peripheral processes of auditory nerve fibers [36]. Intrinsic neurons are intermixed with the principal cells in rodents [37-46]. In other mammals, such as cats, squirrel monkeys, and humans, members of the LOC system may be found outside the LSO in various periolivary nuclei [38,47-51]. The functional significance of the location of these efferent cell bodies is unknown.

The principal neuron is the dominant cell type in the LSO but there are disagreements with respect to the laterality of their ascending projections. They have been qualitatively reported as bilateral and symmetric [27,52-56] or with a contralateral preference [57-60]. There are reports that (1) ipsilateral projections are glycinergic and entirely inhibitory [61,62], (2) ipsilateral projections are primarily low frequency, whereas high

frequency projections are mostly contralateral (cats, [28,63]; and (3) low frequencies project contralaterally, whereas high frequencies project ipsilaterally (ferrets, [29]).

A tonotopic organization has been shown for the LSO [64-67] and IC [68-71]. This organization for the LSO appears dependent on its topographic and tonotopic input from the CN as well as from the MNTB [10,72-74]. The IC gets tonotopic input from the CN [55,75,76]. Topographic and tonotopic connections between the IC and LSO have been reported using large injections of a retrograde tracer in cats [57] and rats [54] but a more detailed analysis of this pathway is merited.

The data on the LSO have been collected under a variety of different conditions, perhaps accounting for some of the disagreements in the literature. The aims of this study in the adult mouse were (1) to address the cell types of the LSO; (2) to determine quantitatively if the projection of principal neurons to the IC is symmetric; and (3) to expand on previous findings of LSO topography and tonotopy.

Methods

Mouse Model of Hearing

This study was performed in strict accordance with the Australian Code for the Care and Use of Animals for Scientific Purposes (2013) and the ethical guidelines of the National Health and Medical Research Council (NHMRC) of Australia. All animals were handled according to Animal Ethics Committee protocols (Animal Research Authority: 19-33, 20-02, and 21-13) and approved by the Garvan/St Vincent's Hospital Animal Ethics Committee. All procedures were conducted under appropriate anaesthesia and analgesia with animal welfare consideration underpinned by the principles of Replacement, Reduction and Refinement. A total of 44 healthy CBA/CaH mice of either sex and between the ages of 3-8 months were used.

Hearing Status

All animals underwent auditory brainstem response testing prior to experimentation. Animals were positioned in a double-walled, sound-attenuating chamber (Sonora Technology, Gotenba, Japan) on a heating pad under ketamine/xylazine (100 mg/kg; 20 mg/kg) anaesthesia. When areflexic to a toe-pinch, the recording, reference, and ground electrodes were positioned beneath the skin above the vertex, left pinna, and biceps femoris, respectively. A speaker was positioned 45˚ off the midline and 10 centimetres from the pinna where alternating condensation and rarefaction click stimuli (100 µsec square wave pulses) and tone stimuli at 4, 8, 16, 24, 32, 40, and 48 kHz (5 ms duration, 0.5 ms rise/fall) were generated using a software-controlled signal processor (RZ6/BioSigRZ; Tucker-Davis Technologies (TDT)) and delivered from 90dB to 30dB SPL in 10dB decremental steps to either ear separately. Stimulus presentations (n=512) were delivered at a rate of 10/s for each level and the evoked responses were amplified (RA16PA/RA4LI; TDT), bandpass filtered from 0.5-3 kHz, recorded, and averaged (RZ6; TDT). Only mice with normal auditory brainstem response thresholds and audiograms [77-79] were used in this study.

Neuronal Tract Tracing

Inferior Colliculus Injections

Injections of retrograde tracers, Fluorescein Dextran (FD-3000MW, biotinylated, 5% in saline; Cat #D3305, Invitrogen/Molecular Probes, Scoresby, VIC, Australia), Fluorogold (FG; 4% in saline, Fluorochrome, Denver, CO), Cholera Toxin Subunit-B (CTB; 0.5% in saline; List Biological Laboratories, Campbell, CA) and Antonia Red Dextran 4 (AR; 10% saline; cat# 79672, Sigma Aldrich, St Louis, Missouri, USA) were made iontophoretically (Supplementary Material 1) or via pressure (up to 0.5 µL) into the central nucleus of the IC. Pressure injections were used in the IC to maximize the labeling of the principal neurons in the LSO, particularly to show their neuronal distribution within the nucleus.

The IC surgical approach began by making a skin incision on the dorsal surface of the head to expose the cranial sutures, bregma and lambda. Approximately 5.2 mm posterior to bregma, a craniotomy (roughly 2 mm^2) was made overlying the IC. A glass micropipette (20-60 µm, inside tip diameter) was positioned on a micromanipulator and used to pressure inject 0.5 µL of tracer (100 nL/min) into the IC at a depth of 1.0-1.5 mm (stereotaxic coordinates of Paxinos and Franklin, [80]). Bilateral injections into each IC were performed with FD and FG to visualize the bilateral projection property of both IC (as above, n=7). Following IC injections, bone wax was applied to cover the craniotomy, and VetBond tissue adhesive was used to close the incision site for the post-surgical survival period. Retrograde tracers were placed in both the IC and cochlea of a mouse (n=4) in order to label LSO neurons with ascending and descending projections in the same LSO.

Cochlea Injections

The surgical approach to the cochlea involved a post-auricular incision and removal of the tympanic membrane and the ossicular chain. With the middle ear opened, a microliter syringe was used to inject 0.5-1 µL of tracer directly into the round window (n=21). After injection, the round window was plugged with bone-wax to prevent tracer leakage, bupivacaine (0.05 mL) was injected subcutaneously at the incision site, and VetBond was used to close the incision. The animal survived 14 days following the injection.

Tissue Processing

Animals were euthanized with an intraperitoneal injection of Lethabarb (0.1 mg/kg) and perfused transcardially with 3-5 mL of 1% sodium nitrate in phosphate-buffered saline, followed by 60 mL of 4% paraformaldehyde (0.1M phosphate buffer, pH 7.4). The head was removed, the calvaria partially opened to expose the brain, and the head post-fixed for two-three hours. The brain was then completely dissected out of the skull and post-fixed overnight at room temperature in 0.1M buffered 4% paraformaldehyde. The next day, the brain was embedded in a

gelatin-albumin mixture hardened with 4% paraformaldehyde and sectioned into 60 μm-thick sections using a vibrating microtome (Leica VT1200S, Nussloch, DE).

Cresyl violet (CV) staining was routinely performed on sections mounted on slides using a protocol modified from Humason (1979). The sections were hydrated in distilled water for 5 minutes, followed by a 10-minute incubation in 0.1% CV dye at room temperature. The slides were rinsed in distilled water, followed by rinses in 70% alcohol, 95% alcohol and then differentiated (95% alcohol with 10 drops of glacial acetic acid) for one minute to remove excess staining. Rehydration in decreasing concentration of alcohol (one-minute periods in 70%, 50%, 30%, and distilled water) further removes excess CV for air-drying overnight and cover slipping with Permount the next day.

Cholinergic Staining

Cholinergic markers, choline acetyltransferase (ChAT; n=7) or acetylcholinesterase (AChE; n=3), were used to visualize the cholinergic neurons of the LSO. The two methods were used to confirm cell counts and size measurements. Immunohistochemical processing of ChAT was performed on free-floating sections. Sections were washed 3x for 5 min each in 0.12M-Tris buffered saline, placed in 3% hydrogen peroxide for 10 minutes, followed by washes with Tris buffered saline, incubated in 0.1% Photoflo (Kodak, Rochester, NY, USA) for one hour, and followed by an hour in 10% normal goat serum. Sections were washed and incubated at 4°C overnight in 1:1000 mouse anti-ChAT primary antibody (Cat #VP- C3838; RRID:AB 2336337; Vector Labs, Newark, CA, USA) and 2% normal goat serum. Negative control sections were unexposed to primary antibody. The following day, sections were rinsed and incubated for one hour in 1:200 biotinylated goat anti-mouse secondary antibody (Cat #BA-9200, Vector Labs, Newark, CA, USA). Sections were rinsed and then developed in a solution of 0.005% 3,3'-diaminobenzene (DAB) with 0.03% hydrogen peroxide until a distinct brown reaction product appeared in the tissue or intensified by the addition of nickel ammonium sulfate

to produce a deep purple reaction product (NiDAB). All sections were mounted and coverslipped with Permount (ThermoFisher, Waltham, MA, USA) for examination by brightfield microscopy.

Cholinergic staining for AChE was performed on glass-mounted tissue sections using a standard protocol [81]. Briefly, the slides were incubated in acetylcholine medium for 30 minutes, followed by 6x 30 second rinses in distilled water, then incubated in 4% sodium sulphide solution for 1 minute, followed by 2x 30 second rinses in distilled water. The tissue was "toned" in 1% silver nitrate for 30 seconds, rinsed 6x 30 sec in distilled water, air dried overnight, and then coverslipped with Permount. LOC cell counts and measurements confirmed labeling equality for ChAT and AChE.

Fluorescent Tracer Processing

All cases with fluorescent tracer injections were visualized with standard fluorescent microscopy. The tissue sections were cut, mounted immediately, and coverslipped with VectaShield (H-1400; Vector Labs, California, USA). In cases where chromogenic processing was performed after fluorescent imaging, the coverslips were removed, and the tissue was processed accordingly.

Immunohistochemical Processing of Neuronal Tracers

Thirteen injection cases with tracer deposits of FG, FD and/or CTB were processed by chromogenic development. Free-floating tissue sections were placed in serial order in 24-well plates. Sections were washed in 0.12M Tris buffered saline, treated with 3% hydrogen peroxide for 10 minutes, rinsed, and permeabilized in 0.1% Photoflo (Kodak, Rochester, NY, USA) for one hour. Tissue processed for biotinylated FD were then incubated for one hour in avidin-biotin complex (Vectastain Elite ABC Kit, Cat# PK-6100; Vector Labs, California, USA) before undergoing development with DAB (as above).

Tissue processed for FG were incubated for one hour in 10% normal goat serum (Cat#VES100020, Vector Labs, California, USA), whereas CTB-tissue was placed in 1% normal rabbit serum (Cat # S-5000; Vector Laboratories, Burlingame, CA). The tissue then underwent 3x rinses for 5 min, before being placed at 4°C overnight in 1:100 rabbit anti-FG primary antibody and 2% normal rabbit serum (Cat#R4880, Sigma Aldrich, St Louis, Missouri, USA) or polyclonal goat anti-CTB primary antibody (1:10,000; Cat# 703, RRID:AB_10013220; List Biological Laboratories) with 2% normal goat serum. Negative control sections were not exposed to primary antibody. FG sections were rinsed and incubated in biotinylated goat anti-rabbit secondary (Cat #AB207995, Abcam, Cambridge, United Kingdom) and CTB sections were incubated in biotinylated rabbit anti-goat secondary (1:200; Cat# BA-5000; Vector Labs) for one hour, rinsed, and incubated for one hour in avidin-biotin complex. Sections were developed with either 0.005% 3,3'-diaminobenzene (DAB) or nickel-intensified DAB (NiDAB). Some cases were counterstained with CV. In cases where two tracers were injected, FD was processed prior to FG. All sections were mounted and coverslipped with Permount for examination with brightfield microscopy.

Quantification of the LSO Neuronal Cohorts and Statistics

Photomontages of serial sections were created from low magnifications (2.5x, 10x and 20x objectives) from the facial nucleus to the ventral nucleus of the lateral lemniscus to identify the boundary of the LSO. Cell measurements of the different neuron types was made from high magnification brightfield and fluorescent micrographs (40x Plan-Apochromat or 100x Neofluar objectives). Micrographs of the LSO was created by making z-stacks from 4-5 focal planes using *Photoshop* software (300 dpi resolution), [82]and the micrographs were pieced together into montages to cover the entire LSO. Only cells with a visible nucleus were included for analysis. The size of principal and intrinsic neurons were compared in male and female mice aged from 3-8 months and the sizes of principal cells, POs, intrinsic cells, and shell neurons were all compared

with respect to the different staining methods. There is no statistical size difference created by age, sex, or staining methods for the data reported (Supplementary Material 2; Supplementary Tables 1, 2, and 3). Positive controls for our cell size method were provided by results calculated from vesicular Glutamate Transporter-2-stained principal cells and AChE-stained intrinsic cells of the Allen Brain Atlas [83]. There was no difference when comparing average somatic areas from our tissue to these other two data sets (vesicular Glutamate Transporter-2: *p=0.2009;* AChE: *p=0.3118, Welch's t test*).

The ratio of ipsilateral and contralateral projecting principal neurons was calculated from bilateral counts of projecting principal neurons from the most rostral to the most caudal LSO sections. The cell body had to be contained inside the fiber-lined border LSO border (principal and intrinsic neurons) or within approximately 100 µm of the LSO boundary (POs and shells). Cell position was plotted onto the outline of the LSO to create maps of cell projection patterns. Somatic silhouette area was calculated using *FIJI* software [84].

The methods for evaluating somatic and dendritic alignment and for confirming cellular alignment to the tonotopic axis are described in Supplementary Material 3 and Supplementary Material 4, respectively. The cell body silhouette area, neuronal counts, angle difference between somatic long axis and dendritic vector, and orientation of LSO neurons to the tonotopic axis were subject to *Descriptive Statistics*, *Welch's t test, and Two-way ANOVA* using *Šídák's Multiple Comparison Test* [85]. *Note*: Statistical analyses that compare two cohorts tested for significance in *Prism* Software using the *Welch's t test*; statical analyses comparing more than two groups were tested for significance using a *Two-way ANOVA* test. Means and standard deviations, *p-values*, and statistical tests are provided.

Results

The goal of this study was to begin a systematic description of some LSO circuits in the mouse in the context of various conflicting reports on the nucleus made in different mammalian

species. We used a range of frequency-defined injection sites to describe the tonotopic relationship between principal cells of the LSO and the IC, applied quantitative methods to determine the laterality of these projections, and re-visited LSO cell categories with a focus on LOC efferents.

Labeling of Principal and Periolivary LSO neurons

Unilateral injections of the retrograde tracers, FD, FG, and/or AR, were made into the CNIC to label LSO neurons with ascending projections (Figure 1). Initially, pressure injections were made to get a global view of the connections, where unilateral injections labeled cells in both the ipsilateral and contralateral LSO (Figure 1A). The labeled neurons were distributed uniformly and appeared homogenous in appearance, except for some neurons on the border of the nucleus. The main neurons exhibited a general orientation towards the dorsal hilus (DH) and fit the descriptions of LSO principal neurons [19,20]. A small number of topographically labeled neurons were located on the border of the nucleus and often conformed to the border's shape; these matched the description of marginal cells [19,20]. Cells with a larger cell body and dendrites that did not exhibit any particular orientation were occasionally labeled and found outside the LSO proper (Figure 1A, arrowheads). These were the PO neurons of the LSO as described in the cat [27,86].

Bilateral injections into the left and right CNIC labeled ipsilateral and contralateral LSO neurons side-by-side throughout the nucleus and were indistinguishable except by tracer (Figure 1B). Principal cells had elongated cell bodies of generally equal size (ipsilateral, 129.3 ± 37.37 μm^2; contralateral 131.2 ± 36.87 μm^2, Supplementary Table 3) with a marked orientation toward the DH. No neurons were double labeled, indicating that a single neuron did not give rise to an ascending axon that innervated both ICs. A much smaller number (<25) of large, multipolar PO cells (198.5 ± 30.2 μm^2, Table 1) were labeled by all IC injections, and these were scattered around the outside of the LSO (Figure 1A, 1B). A comparison of ipsilateral and contralateral principal cell body size and shape can be made and considered with respect to that of POs (Figure 1C).

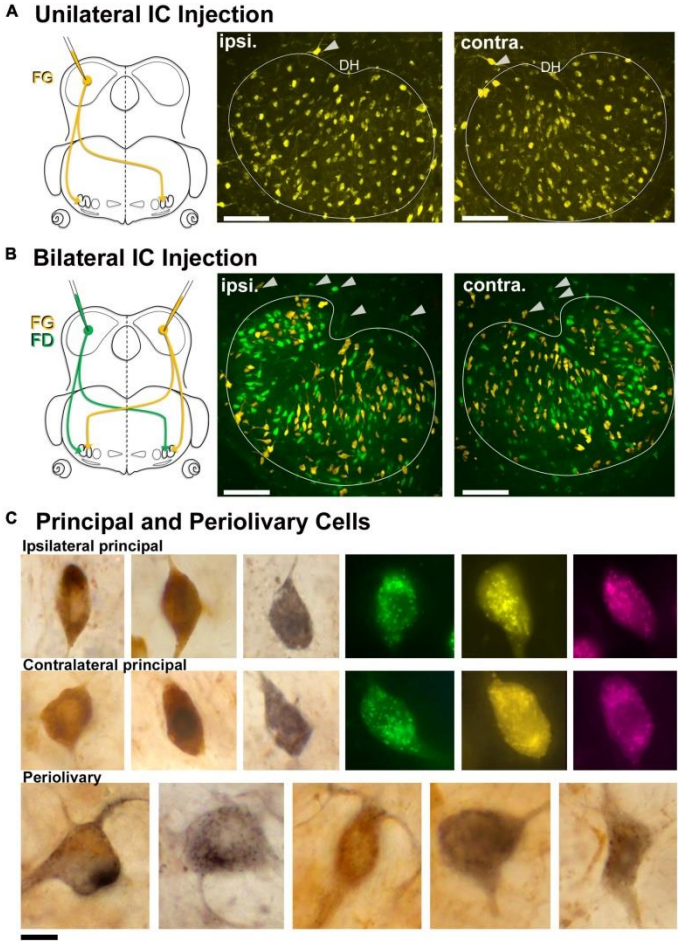

Figure 1: Retrogradely labeled LSO principal neurons from unilateral and bilateral tracer injections into the CNIC.
A. A unilateral injection of a retrograde tracer into the CNIC resulted in bilateral labeling of LSO principal neurons. Schematic representation of FluoroGold (FG) injected into the CNIC to label the neurons in the LSO with ascending projections. Photomicrographs (20x objective) of the ipsilateral and contralateral LSO showing FG-labeled principal neurons. *Grey arrowheads:* PO neurons on the borders of the LSO. **B**. Schematic illustration of the retrograde tracers FG (yellow) and FD (green) injected into the right and left IC, respectively (same animal), to label the principal neurons in the LSO. Photomicrographs (20x objective) of the ipsilateral and contralateral LSO showing FG and FD labeled principal neurons in the same nucleus. *Grey arrowheads:* PO neurons on the borders of the LSO. **C**. Photomicrographs (100x objective) of the ipsilateral (top row) and contralateral (middle row)

principal cells labeled from chromogenic development of FG with DAB (brown) or NiDAB (black) and fluorescent tracers (FD-green, FG-yellow, Antionia Red-magenta). The principal neurons were fusiform with unipolar or bipolar dendritic extensions. The perolivary neurons were also labeled (bottom row) and featured a large, polygonal cell body using chromogenic development. *Abbreviations:* ipsilateral (ipsi.); contralateral (contra.); fluorogold (FG); fluorescein dextran (FD). Scale bar equals 100 µm (A, B), 25 µm (C).

Table 1: Cell body silhouette area (µm2) for the principaland periolivary (PO) neurons and the intrinsic and shell efferent neurons. Two-way testing was used to compare the soma silhouette area of all subtypes of LSO neurons assessed in this study. A two-way ANOVA showed significant differences existed between the principal, PO, intrinsic, and shell neurons, but no significant difference occurred between the CV labeled neurons and the principal neurons ($F(105,438) = 0.86$, $p=0.8408$) or the CV labeled neurons and the intrinsic efferents ($F(1,103) = 3.09$, $p=0.0816$).

***Neurons*:**	**Principal**	**PO**	**Intrinsic**	**Shell**	**Large CV**
Number of cases	3	3	4	4	2
Number of cells	439	41	261	33	166
Median (µm^2)	117.9	199.8	96.61	155.2	107.7
Mean (µm^2) ± St. Dev	123.9 ± 26.56	198.5 ± 30.17	97.33 ± 26.27	161.1 ± 28.26	111.8 ± 37.00

Labeling of LOC Efferents

LOC efferents were labeled by pressure injections of the retrograde tracers FD, FG, or CTB into the round window of the cochlea (Figure 2A). The labeling for intrinsic efferents, found within the LSO proper, was entirely ipsilateral. Labeled cells were oval with thin unipolar or bipolar dendritic stalks generally evident on opposite poles. The intrinsic efferents appeared to align perpendicularly to the borders of the LSO nucleus. Their somata were slightly smaller (97.33 ± 26.27 µm^2, Table 1) than those of principal cells but their shape was roughly the same (Figure 2A and Figure 2B, row 1). A few labeled shell efferents were found bilaterally and outside the LSO borders, often near the DH (Figure 2A, arrowheads). Shell neurons were larger than intrinsic neurons (average area, 161.1 ± 28.3 µm^2, Figure 2B, bottom row; Table 1).

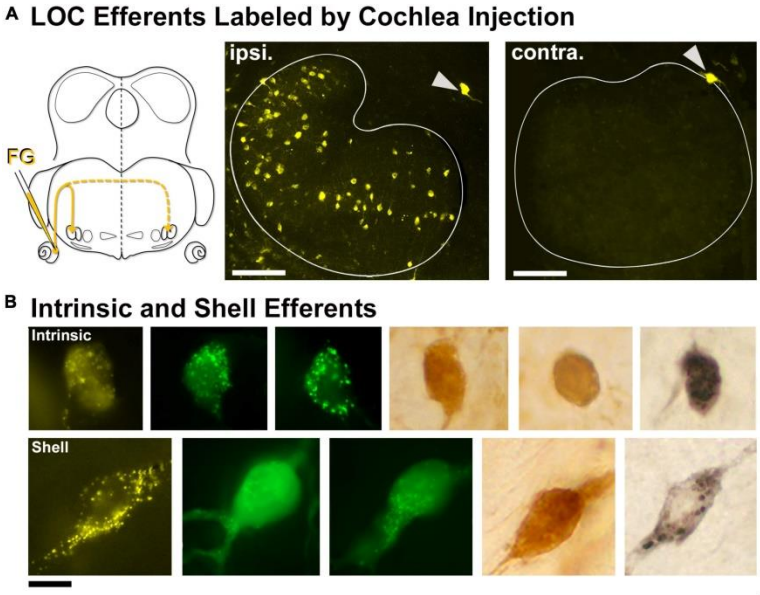

Figure 2: Labeled lateral olivocochlear (LOC) efferents following retrograde tracer injections into the cochlea.
A. Schematic illustration of retrograde tracer injected through the round window of the left cochlea. Solid yellow line indicates the primary pathway to the ipsilateral LOCs, whereas the dashed line leads to the very few contralateral LOCs. *Grey arrowheads:* shell neurons on the borders of the LSO. **B**. Photomicrograph (100x objective) of the intrinsic LOC efferents (top row) labeled with chromogenic development (DAB-brown, NiDAB-black) and with fluorescent markers (FG-yellow, FD-green). The intrinsic neurons were small and round, and look similar to the principal neurons. The shell neurons (bottom row) were labeled in the same tissue as the intrinsic neurons, and featured a large cell body with broader dendritic extensions. *Abbreviations:* ipsilateral (ipsi.); contralateral (contra.); fluorogold (FG); fluorescein dextran (FD). Scale bar equals 100 µm (A), 25 µm (B).

ChAT or AChE was used to determine total efferent cell distribution (Figure 3A) as well as cell morphology (Figure 3B) because they had previously been shown to label LOC efferents in the mouse [42,45]. Intrinsic cells were orientated in line with the tonotopic axis of the LSO (Figure 3A) as previously reported [39,42]. ChAT and AChE staining confirmed that the two methods exhibited equal sensitivity for counting (ChAT: average total, 362.0 ± 25.41; AChE: average total, 357.8 ± 18.63; *p=0.7532;* Table 2) and size measurements (Supplementary

Table 3). Intrinsic efferents had fusiform-shaped cell bodies and the dye often extended into the primary dendrite (Figure 3B, top row). The labeling of the intrinsic and shell neurons with cholinergic staining was consistent with the LOC efferents labeled by retrograde tracers (Figure 3).

Table 3: Counts comparing the distribution between the ipsilateral and contralateral principal neurons of five cases. The number of ipsilateral and contralateral principal neurons were calculated to compare the labeling distribution between both sides. The ratio was computed by dividing the total ipsilateral cells of each case by the total contralateral cells. A ratio closest to 1, infers a labeling distribution that is most comparable between the two sides. The average ratio for these seven cases is 1.05 ± 0.16. *Note:* Cases mentioned more than once were double labeled with FD and FG tracers.

Case	Tracer	Total Ipsilateral Cells	Total Contralateral Cells	Total Count	Ratio
AM1360	FD	362	350	712	1.03
AM1362	FD	812	685	1497	1.18
AM1496	FD	273	232	505	1.17
AM1496	FG	370	382	752	0.969
AM1507	FD	203	263	466	0.772
AM1507	FG	743	589	1332	1.26
AM1526	FG	160	160	320	1

Double labeling experiments were used to reveal principal and intrinsic neurons within the same mouse. An injection of one tracer into the CNIC and an injection of a second tracer into the cochlea on the opposite side permitted direct side-by-side comparisons of principal and intrinsic neurons (Figure 4A). Principal neurons were distributed bilaterally throughout the LSO. In contrast, the intrinsic neurons were unilateral to the cochlear injection and tended to avoid the border of the nucleus. No neuron was double labeled, indicating that no neuron gave rise to a branched axon that innervated the separate targets. When tissue was stained only by CV, it was impossible to distinguish principal from intrinsic cells (Figure 4B). The PO and shell neurons were observed scattered around outside the LSO borders and were always found in association with retrogradely labeled principal and intrinsic neurons, respectively (Figure 4C).

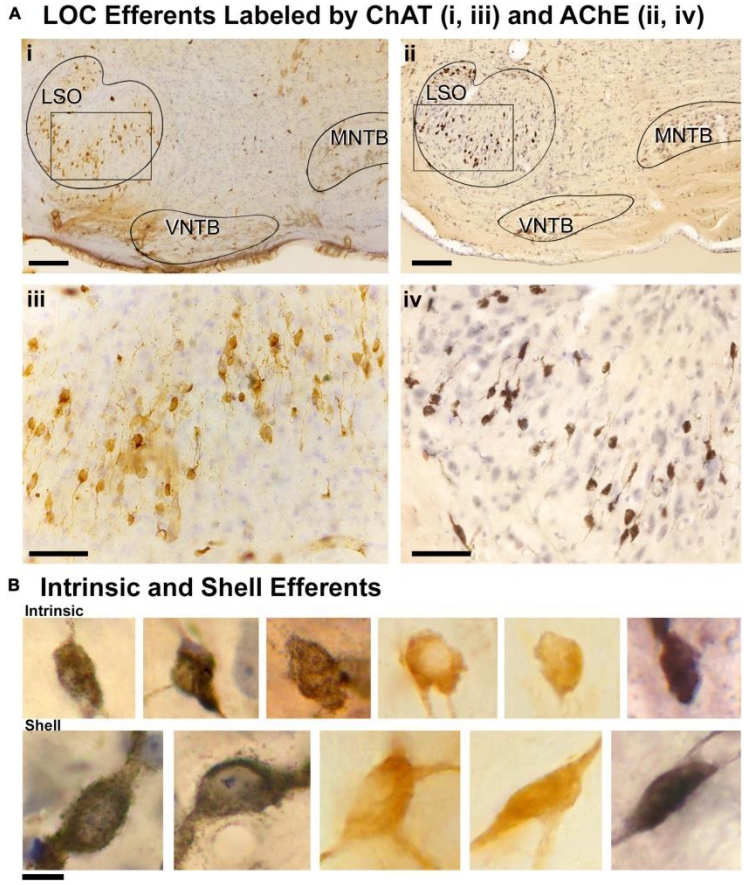

Figure 3: Labeled cholinergic LOC efferent neurons.
LOC neurons were labeled using cholinergic markers, ChAT and AChE, and counterstained with CV. **A.i.** Photomicrograph (10x objective) of the superior olivary complex (SOC) region labeled by ChAT immunostaining. **ii.** Photomicrograph (10x objective) of the SOC region labeled by AChE staining. (**iii, iv**) Higher magnification micrographs (40x objective) of inset **i** and **ii**, showing the ChAT and AChE labeled LOC neurons contained within the LSO, respectively. Note the similarity of ChAT and AChE labeling. B. Photomicrographs (100x objective) showing the cholinergic LOC neurons labeled from either ChAT or AChE staining. The intrinsic neurons (top row) feature fusiform somata and were distributed throughout the core of the LSO nucleus. The shell neurons (bottom row) were larger and more globular in shape. *Abbreviations*: Lateral superior olive (LSO); ventral nucleus of the trapezoid body (VNTB); medial nucleus of the trapezoid body (MNTB). Scale bar equals 250 µm (**Ai,ii**), 50 µm (**Aiii,iv**), 25 µm (**B**).

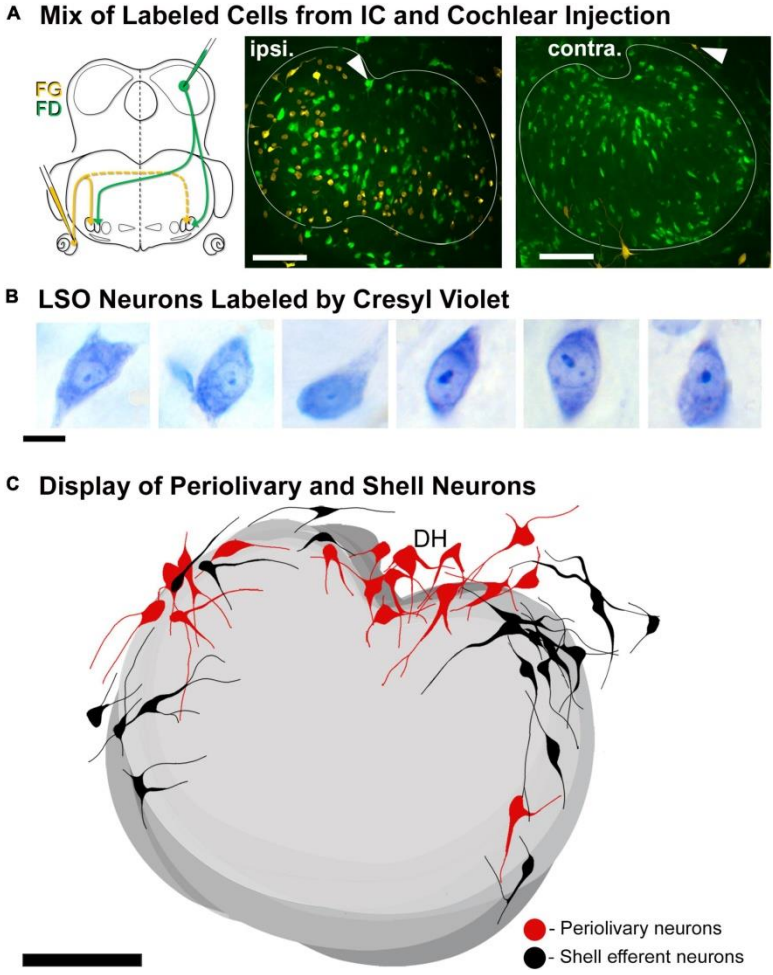

Figure 4: Double injection of retrograde tracers into the right IC and left cochlea to label the LSO neurons with ascending projections and LOC efferents with descending projections, respectively.

LSO neurons with ascending and descending projections were labeled via tracer injections of FD into the right CNIC and FG into the round window of the left cochlea, respectively. **A.** Schematic illustration of the injection sites and pathways for the projecting neurons. Fluorescent micrograph showing the left LSO containing labeled contralateral principal neurons (FD-green) and ipsilateral LOC efferents (FG-yellow). The LOC efferents were primarily ipsilaterally projecting, with only a few shell neurons projecting contralaterally. *Grey arrowheads:* PO neurons (green fluorescence) and shell neurons (yellow fluorescence) on the borders of the LSO. **B.** Photomicrographs (100x objective) of CV labeled LSO neurons. In tissue stained by CV, we were

unable to distinguish principal from intrinsic neurons due to the similarity in size and shape. **C.** Summary of location of labeled periolivary and shell neurons around the borders of the LSO. The position of PO (red) and shell (black) neurons are shown collapsed across 18 LSO sections to illustrate their spatial distribution around the LSO. *Abbreviations:* ipsilateral (ipsi.); contralateral (contra.); fluorogold (FG); fluorescein dextran (FD). Scale bar equals 100 µm (A, C), 25 µm (B).

Topographic Connections between LSO Principal Cells and the CNIC

Thirteen mice received iontophoretic injections of a retrograde tracer into the CNIC at an identified frequency location (Supplementary Figure 1). Four representative cases are shown to illustrate the topography and the bilateral symmetry in the projection (Figure 5). Plots from three adjacent sections were transferred onto the section representing the 50th percentile. The labeled cells occupy a relatively circumscribed region in the LSO. In terms of topography, note how the progressively deeper IC injections with higher frequencies (Figure 5, left column; Figure 6A) create labeling of principal cells in the LSO that move e*n masse* as a "stripe" from lateral to medial (Figure 5, middle columns; Figure 6B). There is also a scattering of labeled PO neurons found just outside the LSO, and these occur in predictably low numbers but in variable locations. The pattern of labeling was similar for all cases and independent of the retrograde tracer used, involving principal, marginal, and PO cells.

The bilateral symmetry of the retrograde labeling was assessed by copying the plot from right 50th percentile of the LSO, flipping the image in the horizontal plane, and then superimposing the flipped image onto the original left LSO (Figure 5, far right column). The mirror imaging of the right and left plots confirms the symmetry. The spatial balance was also evident by the equal numbers of ipsilateral and contralateral labeled cells whose ratio averaged 1.05 ± 0.16 (Table 3).

Table 2: Counts comparing the distribution of LOC efferents stained by AChE or ChAT. The number of LOC efferent neurons were calculated to compare the labeling distribution between the two stains. The average count for AChE and average count for ChAT were not significantly different (*p=0.7532*).

Case	Stain	Count
AM4	AChE	343
AM5	AChE	344
AM11	AChE	389
AM298	AChE	331
AM1348	ChAT	385
AM1351	ChAT	380
AM1353	ChAT	382
AM1417	ChAT	376
AM1419	ChAT	331
AM1450	AChE	354
AM1454	AChE	355
AM1477	ChAT	349
Average AChE	357.8 ± 18.63	
Average ChAT	362.0 ± 25.41	
Combined average	359.9 ± 21.35	

While the "sheets" of labeled cells exhibit a tonotopic organization, there is also spatial overlap of principal cells that exhibited separate but similar frequency characteristics (Figure 6B). This overlap of labeled cells in the LSO reflects the overlap observed in the IC injection sites having different but nearby frequency characteristics (Figure 6A). The spatial spread in the distribution of labeling may be a result of combining data from different cases onto a model LSO. PO cell labeling was relatively invariant, regardless of the location of the IC injection (Figure 5, middle columns). Every part of the CNIC appears innervated by both populations of cells with principal and marginal cells having restricted projections and PO cells having widespread projections.

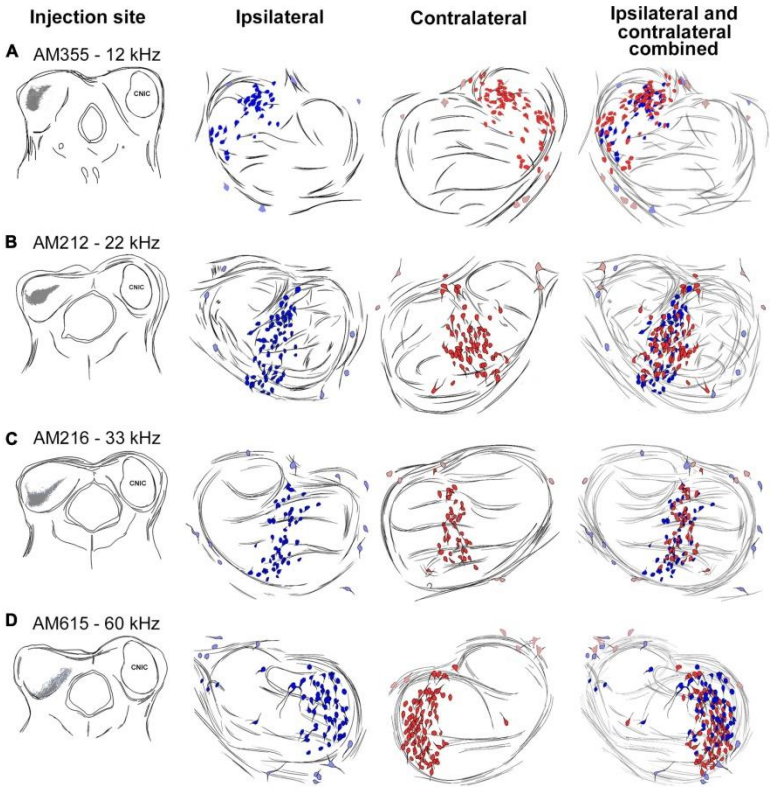

Figure 5: Topographic relationship between the IC and the LSO.
Tracing of IC injection sites progressing more ventral and higher in frequency (**A-D**, left column). The corresponding bilateral labeling of LSO principal cells (ipsilateral-dark blue, contralateral-dark red, middle two columns) and periolivary (PO) cells (ipsilateral-light blue, contralateral-light red) were traced through serial sections, aligned using blood vessels, and merged. The ipsilateral and contralateral labeling for each injection was combined (last row) to show the bilateral preservation of topographic and tonotopic organization of principal cells across the LSO. PO cells do not observe a tonotopic distribution (light blue and red). *Abbreviation*: kilohertz (kHz).

Tonotopic Axis

The angle of the somatic long axis compared to the corresponding angle of its dendritic vector for principal and intrinsic neurons was small, indicating alignment of these two features: (principal cells: 7.24 ± 10.42˚; intrinsic efferents: 6.49 ± 9.33˚; Supplementary Table 4). This result inferred that the cell body pointed in the direction of the dendritic trajectory

(further details in Supplementary Material 3) and allowed us to quantify the somatic orientation of LSO cells to the tonotopic axis (Supplementary Material 4).

The principal cells created a columnar profile that defined an "isofrequency" sheet (Figure 5, 6B) that ran the length of the LSO, hinged near the DH. An isofrequency sheet for each case was laid out on the 50th percentile of the nucleus (Figure 6C). A centroid was calculated for each isofrequency sheet (FIJI) and black vertical lines were drawn through the centroids to create a long axis line for each sheet (Figure 6C). The centroids were connected by a black line that represented the tonotopic axis of the nucleus (Figure 6D).

The Hamilton-Jacobi Skeleton algorithm [87], which bisects a complex structure by following the curvature of the opposing borders, was used to create a representative tonotopic axis line for 14 LSO sections (Figure 6D, red lines). This output closely matched the tonotopic axis defined by us (Figure 6D, black line; *Welch's test (p=0.2967*)). The spatial representation of different isofrequency regions appear uniformly distributed across the LSO, at least up to 60kHz, suggesting no augmented frequency representation. A line through the 30kHz region would essentially bisect the LSO into lateral and medial halves.

The somatic long axes of principal and intrinsic neurons were placed onto our LSO model (Supplementary Material 4) and the intersecting angle θ was measured with respect to the tonotopic axis. As suggested from the literature, LSO neurons are expected to be oriented at right angles to the tonotopic axis [88,89]. Each angle was reported as an absolute value and subtracted from 90˚. Principal and intrinsic neurons exhibited a somato-dendritic orientation that aligned to one another and was mostly orthogonal to the tonotopic axis (Figure 7; principal neuron mean of all LSO sections = 32.99 ± 24.55˚; intrinsic neuron mean = 29.70 ± 22.51˚). The arrangement was not perfect but the tendency was definitely present. The PO neurons and shell efferents, however, exhibited somato-dendritic morphology that did not contribute to the structural laminae (middle, PO mean = 61.28 ± 24.62˚; shell efferent mean = 59.71 ± 24.39˚, Supplementary Table 5). These measurements

confirmed the more orthogonal appearance of these two cell types with respect to the tonotopic axis of the LSO.

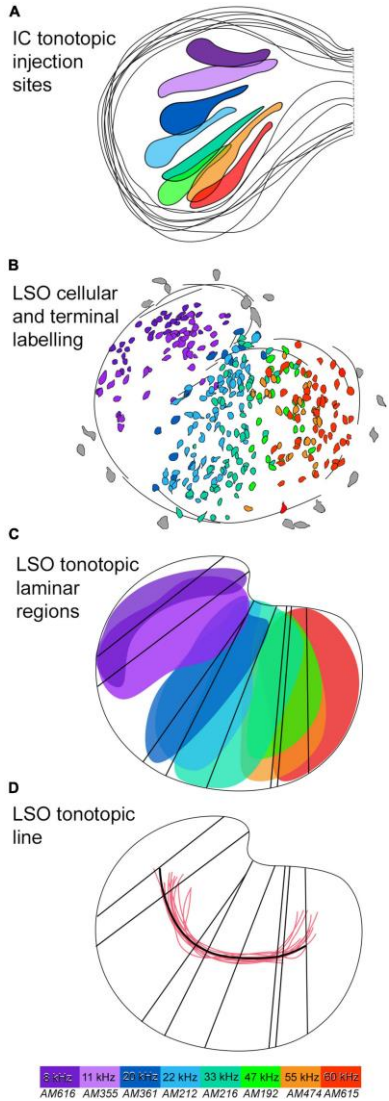

Figure 6: Tonotopic relationship between the IC and LSO with a tonotopic axis.

A. Several IC injections were made in the dorsal to ventral regions of the CNIC to labeled the correspondingly low to high frequency output in the LSO. 8 IC injection sites were drawn and superimposed to present an IC frequency representation. Frequencies included: 8 kHz, 11 kHz, 20 kHz, 22 kHz, 33

kHz, 47 kHz, 55 kHz, 60 kHz (colour coded). **B,** The corresponding label of principal neurons in the LSO, colour coded to match. The labeled principal cells show the LSO low to high frequency organisation progressing from the lateral to medial limb, respectively. **C.** The corresponding LSO neurons labeled from each IC injection were colour coded. A region for each colour of principal cells representing one frequency was drawn by outline the area of labeled cells to form a lamina for each frequency. A line representing the long axis of each frequency region was drawn to represent an isofrequency line. **D.** A line (black) representing the tonotopic axis was drawn by connecting centroids of all the isofrequency lines and was compared to other tonotopic axis lines (red) derived from the Hamilton Jacobi output from other LSO sections. A color map is included, with purple corresponding to labeled elements from 8kHz, and red corresponding to the highest frequency elements of 60 kHz. *Abbreviations:* inferior colliculus (IC); lateral superior olive (LSO); kilohertz (kHz).

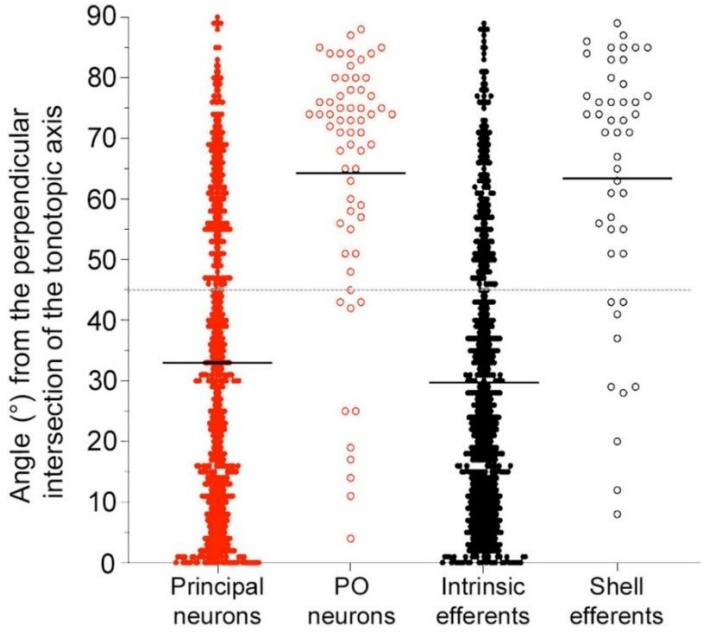

Figure 7: Plot of the angles for LSO neurons with ascending (red) or descending (black) projecting axons with respect to the tonotopic axis.
Angle measurements for the four types of LSO neurons are shown and combined from three regions of the LSO (rostral, middle, and caudal sections). The average angle (black line) was presented for all subtypes. *Gray dashed line:* 45-degree threshold. Principal and intrinsic neurons illustrate similar angle deviations, with mean alignment below the 45-degree threshold across all planes. Periolivary (PO) neurons and shell efferent neurons both had values above the 45-degree threshold for all planes. Smaller values indicate alignment with the frequency organization. *Abbreviation:* periolivary (PO).

Discussion

The present study provides a qualitative and quantitative anatomical assessment of four types of LSO projecting neurons with connections with the IC or cochlea. Retrograde tracers placed into the CNIC labeled neurons with ascending projections (principal and PO neurons), whereas neurons with descending projections were labeled by injections of retrograde tracers deposited into the cochlea or with cholinergic markers (intrinsic and shell LOC efferents). The projection laterality of the principal neurons to the IC was determined by comparing the number of ipsilateral and contralateral labeled neurons from unilateral IC injections and found to be essentially equal. The tonotopic alignment of the four subtypes of LSO neurons was examined and quantified to develop ideas about frequency specificity and possible frequency enhancement with regard to connections between the LSO and the IC. Features of somatic morphology were established to supplement connectivity data and to help distinguish principal and intrinsic neurons. These data are summarized in Figure 8.

In the mouse, principal and intrinsic neurons are spatially intermixed and have similar somatic size, shape, and dendritic morphology. Collectively, these neurons give the LSO a laminar texture and are structurally specialized to receive restricted input, which endows each with a well-defined receptive field. These cells are typical of classic lemniscal sensory neurons [90-92].

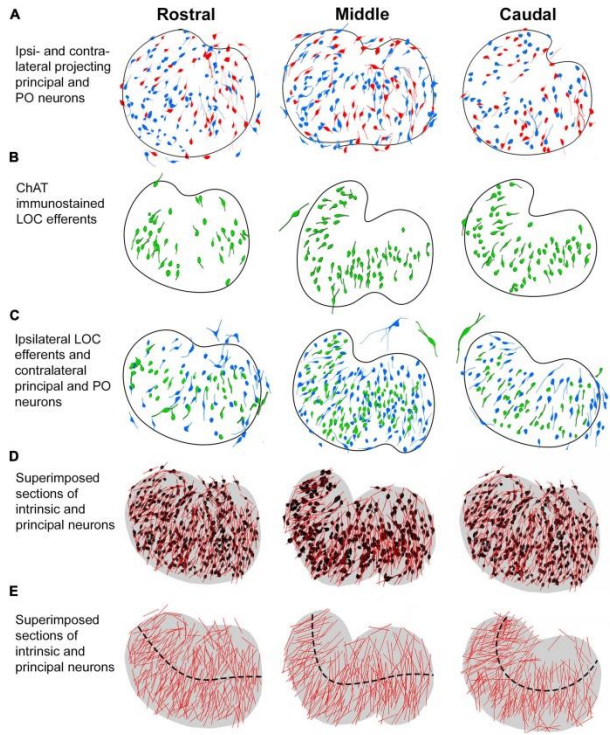

Figure 8: Summary of labeling pattern of principal and intrinsic neurons in rostral, middle, and caudal LSO sections.
The projecting cell types were traced and mapped to illustrate their distribution in representative anterior-posterior regions of the nucleus. **A**. Ipsilateral (red) and contralateral (blue) principal neurons labeled from bilateral CNIC injections. **B.** Intrinsic efferent neurons labeled by ChAT immunostaining (green). **C.** Contralateral projecting principal neurons (blue) and ipsilateral projecting intrinsic neurons (green) labeled by retrograde tracer injections into the CNIC and cochlea, respectively. The larger neurons on the borders of the LSO are identified as the PO and shell neurons (seen in A, B, C). **D**. LSO neurons with ascending or descending projections labeled from separate LSO sections were superimposed and collapsed as one color (black) on a representative rostral, middle, and caudal LSO section. The somatic long axis line (red) is contrasted against the individual neurons. **E.** A model LSO representing rostral, middle, and caudal sections was drawn (gray, fourth row). Here, the relative alignment of principal and intrinsic neurons are shown with the representative tonotopic axis (black dashed line). An overall organization within the nucleus is seen to comprise fibrodendritic laminae. *Abbreviations:* periolivary (PO); lateral olivocochlear (LOC).

LSO Principal Neurons: Projection Symmetry and Topography

LSO cells have been divided into separate categories based on soma-dendritic features, cell body size, and location within the LSO nucleus [19,20,23], chemical markers [25,26] or projections [27-29]. There is general agreement as to the main types of neurons—principal, periolivary, intrinsic, and shell— but not for all. The previously mentioned marginal cells, with their bipolar appearance and topographic relationship with the IC, may simply be principal cells that lie on the borders of the LSO [19,23]. Bipolar, unipolar, and banana-like cells of the rat exhibit disk-shaped dendritic trees and may also represent different subgroups of principal cells with variations in location and chemistry [23]. LSO cell taxonomy is confounded by observations drawn from different species of different ages using different methods. The resolution of cell types will ultimately depend on their physiological properties and the nature of the synaptic circuits to which they belong.

We demonstrated a strict topographic projection from the LSO to the IC, which augmented previous but less detailed reports in cats and rats [54,57]. Our isofrequency layers of the IC closely corresponded to tonotopic maps where isofrequency lines were drawn by connecting points of common frequencies [71,93]. The congruency of these isofrequency layers is remarkable given that these maps were generated years apart by different methods, using different mouse strains, exposed to surgical perturbations and electrode penetrations, and subject to tissue stress by histological processing (Supplementary Material 5).

Following our frequency-guided unilateral IC injections, there are unlabeled cells among the frequency-dependent labeled cells. Some of the unlabeled cells would be principal cells projecting to the other IC and others would be intrinsic efferents [94]. Still others could have projections to different nuclei such as the nuclei of the lateral lemniscus, AVCN and dorsal cochlear nucleus [28,95]. There was also more spatial overlap of cells from different frequency zones than expected when combining data from different cases onto an LSO model. These border

irregularities might simply reflect the combining of data across different animals. Alternatively, they could imply that the system is inherently noisy because it reflects the naturally occurring acoustic environment. That is, we rarely, if ever, encounter pure tones. Rather, we hear complex sounds such as speech, with time-varying frequencies and amplitudes, in the presence of random noises, all occurring at once and from different sources. Could it be that sound perception and discrimination are learned probability functions rather than a precise hard-wired process like the keyboard of a piano? Maybe topographic brain maps are only approximate blueprints for brain function: the auditory world is uniquely created for each individual animal by populations of neurons that learn to work together over time. Their frequency preference is acquired by their relative position in the auditory system and refined by experience but perhaps not dictated entirely by innate and immutable frequency-specific responses.

The pattern of labeled neurons in the ipsilateral and contralateral LSO following a unilateral injection of a retrograde tracer into the mouse IC was not only topographic but also symmetric. If we assume that ipsilateral and contralateral projecting neurons have similar uptake and transport efficiency for detectability, then we could anticipate that the ratio of ipsilateral versus contralateral projecting cells, regardless of the size of the injection, ought to be stable, at least for injections contained within the same IC subdivisions. On average, an equal number of labeled principal cells were reliably observed in each LSO from a unilateral injection in the CNIC (1.05 ± 0.16). The gerbil, in spite of considerable variability, exhibited a similar mean ratio (0.94 ± 0.59, Mellott et al., [60]) consistent with qualitative conclusions made for cats [27], ferrets [29], and rats [96,97]. Other researchers reported differences in ipsi- versus contra-projections and these could be due to species differences or methods. Part of the difference could also be that the tracers being used currently are significantly more sensitive than horseradish peroxidase, which was used in many of the older publications.

The neurons lying outside the LSO with larger somata, multipolar dendrites, and ascending projections to the IC are analogous to the PO neurons in cats [27,85] and gerbils [98]. POs tended to be concentrated around the DH but could be found anywhere in the vicinity of the LSO and connected to the ipsilateral or contralateral IC but not to both. Some members of this population labeled with every IC injection but their numbers were relatively low and their location unpredictable. This pattern of labeling suggested a diffuse projection to the IC and their widely branching dendrites seemed suited to intercept input from a wide swath of incoming fibers.

The POs represent what had been called isodendritic neurons commonly found in the brain stem reticular system or the intralaminar (posterior) nuclei of the thalamus [99-102]. Such cells receive anatomically heterogeneous input from the spinal cord and medial lemniscus [103,104], demonstrate wide receptive field properties [105-107], exhibit distinct neurochemical differences [103], and have been considered part of a multimodal pathway for integrative functions [108]. Could POs be part of the non-lemniscal sensory system? Regardless, these anatomical data imply sensitivity to a range of different kinds of inputs and projections that exert a more modulatory upstream influence.

Labeling of LSO Neurons with Descending Projections

Intrinsic neurons of the mouse exhibit bipolar morphology that resembles that of the principal neurons. They have also been shown to have restricted terminations in the inner hair cell region of the ipsilateral cochlea [109]. In contrast, shell neurons have larger cell bodies and exhibit multipolar, radiating dendrites. Importantly, evidence supports the notion that shell neurons give rise to branching axons with generally a bidirectional course along the cochlear spiral with *en passant* and terminal swellings extending a tonotopic range of 1-2 octaves [109-111]. The diffuse and expansive projections of shell neurons are consistent with characteristic attributed to polysensory, non-lemniscal cells [92,100,112,113].

Long-term acquired hearing loss does not affect the size, number, or ratio of ipsilateral:contralateral projecting OC efferent neurons when comparing CBA/CaH, DBA/2 and shaker-2 (sh2/sh2) mice at 6 months of age [114]. Both DBA/2 and sh2/sh2 mice exhibited ABR thresholds exceeding 100dB SPL at this age. From these observations and the relatively short post-surgical survival of our animals, we infer that our tracer injections into the cochlea did not alter the somatic structure of auditory efferents as seen through a light microscope.

Considerations of LSO Laminar Organization and Tonotopy

The concept of a laminar organization of auditory structures [115] fostered the idea for a topologic representation of isofrequency layers that underpinned tonotopy [10,14,64,65,69,72-74,76,116-121]. Previous studies utilised qualitative observations with Golgi staining to label the extensive dendritic branches of LSO neurons and suggested a laminar organisation that appeared perpendicular to the tonotopic axis [20,22,39,74,89,121,124]. The utility of quantitative analyses using vectors and angles demonstrated a laminar organisation of LSO neurons in the human [124] and a nonlaminar organization of MOC neurons in the mouse [125]. We extended these observations by showing principal and intrinsic neurons conform to the laminar organization of the LSO, whereas PO and shell neurons do not. The observation that MOCs are sharply tuned [126] even though they are multipolar with radiating dendrites [125] implies that frequency-specific inputs are concentrated on the cell body or proximal dendrites, not along the entire dendritic domain.

In the LSO, principal cells contribute to the isofrequency organization and are sharply tuned [65,66,127,128]. In the LSO of the mouse, principal and intrinsic neurons adopt a strict laminar organization, project in different directions, and are predicted to exhibit sharp tuning although physiological recordings have not been made from LOC neurons (Guinan, 2011). Another enigma about LOCs is that in many species, they are located outside of the LSO [47,50]. The predominantly

ipsilateral projecting efferents in the squirrel monkey have small, round-oval somata that could represent LOCs. The elongated neurons that exhibited bilateral projections were embedded in surrounding fibers of the SOC [50]; their projection pattern and fibrodendritic alignment make them candidates for the sharply tuned MOCs.

Comparative Issues of the LSO

There is no uniform agreement with respect to the neurochemistry of LSO neurons, due in part to species variations in cellular composition, cell body versus terminal staining, age of animals studied, and history of noise exposure [25,26,34,39,129-134]. For the cat and guinea pig, the LSO cell population seems to be almost equally divided between excitatory and inhibitory cells [25,135]. In the gerbil, 75% of the LSO cells are reported to be glutamatergic [60]. The projections of LSO principal neurons to the IC have been considered a key to understanding the role of excitation and inhibition in the process of binaural interactions but there is disagreement concerning many of the very basic issues of the circuitry. Different species exhibit variable immunochemical properties of LSO neurons and variations in the laterality of projections with respect to frequency and transmitter [28,29,61-63,135-137]. Projections of the LSO to the IC are not distinguishable by glycinergic or glutamatergic features alone [60,96]. Sorting out the details of these projections in different species will be important to understand the cellular mechanisms of binaural level processing and warrants separate studies that focus on excitation and inhibition by using pathway tracing, synaptic analyses, and markers for glycine and glutamate.

The mouse has primarily high frequency hearing, unlike that of the cat, ferret, chinchilla, gerbil, guinea pig, and human. It can therefore be predicted that there will be anatomical specializations associated with the animal's natural history, ecological niche, hearing range, and conspecific communication requirements. In rodents, for example, the known natural habitat of the gerbil is an underground burrow [138]; it should not be surprising if its LSO differs from rodents living above-ground.

In burrows, there is reduced propagation of high frequencies [138] and little opportunity for detecting lateralized sounds [140,141]. It is, however, curious that three burrowing rodents, the gerbil, mountain beaver, and naked mole rat, have vastly different audible hearing ranges [139,142,143]. In comparison, the mouse lives in open fields and urban developments and has high frequency hearing to assist in conspecific communication and danger detection [144,145]. Our results provide new quantitative details on the auditory anatomy of the mouse but emphasize the importance of comparative studies if we are to better our understanding of mammalian hearing.

References

1. Young ED, Spirou GA, John JR, Herbert FV. Neural organization and responses to complex stimuli in the dorsal cochlear nucleus. Philosophical Transactions of the Royal Society of London. Series B: Biological Sciences. 1992; 336: 407–413.
2. Joris PX. Envelope coding in the lateral superior olive. II. Characteristic delays and comparison with responses in the medial superior olive. Journal of Neurophysiology. 1996; 76: 2137–2156.
3. Joris PX, Yin TCT. Envelope Coding in the Lateral Superior Olive. III. Comparison With Afferent Pathways. Journal of Neurophysiology. 1998; 79: 253–269.
4. Konishi S, Yuille AL, Coughlan JM, Song Chun Zhu. Statistical edge detection: learning and evaluating edge cues. IEEE Transactions on Pattern Analysis and Machine Intelligence. 2003; 25: 57–74.
5. Reiss LAJ, Young ED. Spectral Edge Sensitivity in Neural Circuits of the Dorsal Cochlear Nucleus. Journal of Neuroscience. 2005; 25: 3680–3691.
6. Middlebrooks J. UC Irvine UC Irvine Previously Published Works Title Sound localization. Permalink Journal Publication Date. 2015.
7. Franken TP, Joris PX, Smith PH. Principal cells of the brainstem's interaural sound level detector are temporal differentiators rather than integrators. eLife. 2018; 7: e33854.

8. Joris PX, van der Heijden M. Early Binaural Hearing: The Comparison of Temporal Differences at the Two Ears. Annual Review of Neuroscience. 2019; 42: 433–457.
9. Cant NB, Casseday JH. Projections from the anteroventral cochlear nucleus to the lateral and medial superior olivary nuclei. The Journal of Comparative Neurology. 1986; 247: 457–476.
10. Doucet JR, Ryugo DK. Axonal pathways to the lateral superior olive labeled with biotinylated dextran amine injections in the dorsal cochlear nucleus of rats. The Journal of Comparative Neurology. 2003; 461: 452–465.
11. Warr WB. Fiber degeneration following lesions in the anterior ventral cochlear nucleus of the cat. Experimental Neurology. 1966; 14: 453–474.
12. Tolbert LP, Morest DK, Yurgelun-Todd DA. The neuronal architecture of the anteroventral cochlear nucleus of the cat in the region of the cochlear nerve root: Horseradish peroxidase labelling of identified cell types. Neuroscience. 1982; 7: 3031–3052.
13. Glendenning KK, Hutson KA, Nudo RJ, Masterton RB. Acoustic chiasm II: Anatomical basis of binaurality in lateral superior olive of cat. The Journal of Comparative Neurology. 1985; 232: 261–285.
14. Banks M, Smith P. Intracellular recordings from neurobiotin-labeled cells in brain slices of the rat medial nucleus of the trapezoid body. The Journal of Neuroscience.1992; 12: 2819–2837.
15. Henkel CK, Gabriele ML. Organization of the disynaptic pathway from the anteroventral cochlear nucleus to the lateral superior olivary nucleus in the ferret. Anatomy and Embryology. 1999; 199: 149–160.
16. Yin TCT, Smith PH, Joris PX. Neural Mechanisms of Binaural Processing in the Auditory Brainstem. Comprehensive Physiology. 2019; 1503–1575.
17. Tollin DJ. The Lateral Superior Olive: A Functional Role in Sound Source Localization. The Neuroscientist. 2003; 9: 127–143.
18. Middlebrooks JC, Waters MF. Spatial Mechanisms for Segregation of Competing Sounds, and a Breakdown in Spatial Hearing. Frontiers in Neuroscience. 2020; 14.

19. Ollo C, Schwartz IR. The superior olivary complex in C57BL/6 mice. American Journal of Anatomy. 1979; 155: 349–373.
20. Cant NB. The fine structure of the lateral superior olivary nucleus of the cat. The Journal of Comparative Neurology. 1984; 227: 63–77.
21. Helfert RH, Schwartz IR. Morphological evidence for the existence of multiple neuronal classes in the cat lateral superior olivary nucleus. The Journal of Comparative Neurology. 1986; 244: 533–549.
22. Helfert RH, Schwartz IR. Morphological features of five neuronal classes in the gerbil lateral superior olive. American Journal of Anatomy. 1987; 179: 55–69.
23. Rietzel HJ, Friauf E. Neuron types in the rat lateral superior olive and developmental changes in the complexity of their dendritic arbors. The Journal of Comparative Neurology. 1998; 390: 20–40.
24. Kulesza RJ. Cytoarchitecture of the human superior olivary complex: Nuclei of the trapezoid body and posterior tier. Hearing Research. 2008; 241: 52–63.
25. Helfert RH, Bonneau JM, Wenthold RJ, Altschuler RA. GABA and glycine immunoreactivity in the guinea pig superior olivary complex. Brain Research. 1989; 501: 269–286.
26. Eybalin M. Neurotransmitters and neuromodulators of the mammalian cochlea. Physiological Reviews. 1993; 73: 309–373.
27. Adams J. Ascending projections to the inferior colliculus. The Journal of Comparative Neurology. 1979; 183: 519-538.
28. Glendenning KK, Masterton RB. Acoustic chiasm: efferent projections of the lateral superior olive. The Journal of Neuroscience. 1978; 3: 1521–1537.
29. Henkel CK, Brunso-Bechtold JK. Laterality of superior olive projections to the inferior colliculus in adult and developing ferret. The Journal of Comparative Neurology. 1996; 331: 458–468.
30. Kulesza RJ. Cytoarchitecture of the human superior olivary complex: Medial and lateral superior olive. Hearing Research. 2007; 225: 80–90.

31. Ryugo DK, Fekete DM. Morphology of primary axosomatic endings in the anteroventral cochlear nucleus of the cat: A study of the endbulbs of Held. The Journal of Comparative Neurology. 1982; 210: 239–257.
32. Romand R. Developoment in the frequency selectivity of auditory nerve fibers in the kitten. Neuroscience Letters. 1983; 35: 271-276.
33. Brugge JF. Stimulus coding in the developing auditory system. In: Edelman GM, Gall WE, Cowan WM, editors. Auditory Function: Neurobiological Bases of Hearing. New York: Wiley. 1988; 113-136.
34. Jenkins SA, Simmons DD. GABAergic neurons in the lateral superior olive of the hamster are distinguished by differential expression of gad isoforms during development. Brain Research. 2006; 1111: 12–25.
35. Van Hooser SD. Similarity and Diversity in Visual Cortex: Is There a Unifying Theory of Cortical Computation? The Neuroscientist. 2007; 13: 639–656.
36. Warr WB, Guinan JJ. Efferent innervation of the organ of corti: two separate systems. Brain Research. 1979; 173: 152–155.
37. White JS, Warr BW. The dual origins of the olivocochlear bundle in the albino rat. The Journal of Comparative Neurology. 1983; 219: 203–214.
38. Aschoff A, Ostwald J. Different origins of cochlear efferents in some bat species, rats, and guinea pigs. The Journal of Comparative Neurology. 1987; 264: 56–72.
39. Vetter DE, Mugnaini E. Distribution and dendritic features of three groups of rat olivocochlear neurons. Anatomy and Embryology. 1992; 185: 1–16.
40. Yao W, Godfrey DA. Immunohistochemistry of muscarinic acetylcholine receptors in rat cochlear nucleus. Hearing Research. 1995; 89: 76–85.
41. Campbell JP, Henson MM. Olivocochlear neurons in the brainstem of the mouse. Hearing Research. 1988; 35: 271–274.
42. Brown MC. Anatomy of Olivocochlear Neurons. In: Ryugo DK, Fay RR, Popper AN, editors. Auditory and Vestibular Efferents. Berlin: Springer. 2011; 17-33.

43. Romero GE, Trussell LO. Distinct forms of synaptic plasticity during ascending vs descending control of medial olivocochlear efferent neurons. eLife. 2021; 10.
44. Sánchez-González MA, Warr W Bruce, López DE. Anatomy of olivocochlear neurons in the hamster studied with FluoroGold. Hearing Research. 2003; 185: 65–76.
45. Safieddine S, Wenthold RJ. The Glutamate Receptor Subunit δ1 Is Highly Expressed in Hair Cells of the Auditory and Vestibular Systems. The Journal of Neuroscience. 1997; 17: 7523–7531.
46. Mulders WHAM, Robertson D. Dopaminergic olivocochlear neurons originate in the high frequency region of the lateral superior olive of guinea pigs. Hearing Research. 2004; 187: 122–130.
47. Warr WB. Olivocochlear and vestibular efferent neurons of the feline brain stem: Their location, morphology and number determined by retrograde axonal transport and acetylcholinesterase histochemistry. The Journal of Comparative Neurology. 1975; 161: 159–181.
48. Brown MC, Liberman MC, Benson TE, Ryugo DK. Brainstem branches from olivocochlear axons in cats and rodents. The Journal of Comparative Neurology. 1988; 278: 591–603.
49. Bishop AL, Henson OW. The efferent cochlear projections of the superior olivary complex in the mustached bat. Hearing Research. 1987; 31: 175–182.
50. Thompson GC, Thompson AM. Olivocochlear neurons in the squirrel monkey brainstem. Journal of Comparative Neurology. 1986; 254: 246-258.
51. Moore JK. Organization of the human superior olivary complex. Microscopy Research and Technique. 2000; 51: 403–412.
52. Schweizer H. The connections of the inferior colliculus and the organization of the brainstem auditory system in the greater horseshoe bat (Rhinolophus ferrumequinum). The Journal of Comparative Neurology. 1981; 201: 25–49.
53. Nordeen KW, Killackey HP, Kitzes LM. Ascending auditory projections to the inferior colliculus in the adult gerbil,Meriones unguiculatus. The Journal of Comparative Neurology. 1983; 214: 131–143.

54. Kelly JB, Liscum A, van Adel B, Ito M. Projections from the superior olive and lateral lemniscus to tonotopic regions of the rat's inferior colliculus. Hearing Research. 1998; 116: 43–54.
55. Ross LS, Pollak GD, Zook JM. Origin of ascending projections to an isofrequency region of the mustache bat's inferior colliculus. The Journal of Comparative Neurology. 1988; 270: 488–505.
56. Grothe B. Interaction of excitation and inhibition in processing of pure tone and amplitude-modulated stimuli in the medial superior olive of the mustached bat. Journal of Neurophysiology. 1994; 71: 706–721.
57. Brunso-Bechtold JK, Thompson GC, Masterton RB. HRP study of the organization of auditory afferents ascending to central nucleus of inferior colliculus in cat. The Journal of Comparative Neurology. 1981; 197: 705–722.
58. Willard FH, Martin GF. Collateral innervation of the inferior colliculus in the North American opossum: A study using fluorescent markers in a double-labeling paradigm. Brain Research. 1984; 303: 171-182.
59. Moore DR, Russell FA, Cathcart NC. Lateral superior olive projections to the inferior colliculus in normal and unilaterally deafened ferrets. The Journal of Comparative Neurology. 1995; 357: 204–216.
60. Mellott JG, Dhar M, Mafi A, Tokar N, Winters BD. Tonotopic distribution and inferior colliculus projection pattern of inhibitory and excitatory cell types in the lateral superior olive of Mongolian gerbils. Journal of Comparative Neurology. 2021; 530: 506–517.
61. Saint Marie RLS, Ostapoff EM, Morest DK, Wenthold RJ. Glycine-immunoreactive projection of the cat lateral superior olive: Possible role in midbrain ear dominance. The Journal of Comparative Neurology. 1989; 279: 382–396.
62. Saint Marie RL, Baker RA. Neurotransmitter-specific uptake and retrograde transport of [3H]glycine from the inferior colliculus by ipsilateral projections of the superior olivary complex and nuclei of the lateral lemniscus. Brain Research. 1990; 524: 244–253.

63. Oliver DL. Ascending efferent projections of the superior olivary complex. Microscopy Research and Technique. 2000; 51: 355–363.
64. Boudreau JC, Tsuchitani C. Cat superior olive S-segment cell discharge to tonal stimulation. Contributions to sensory physiology. 1970; 4: 143-213.
65. Guinan JJ, Norris BE, Guinan SS. Single Auditory Units in the Superior Olivary Complex: II: Locations of Unit Categories and Tonotopic Organization. International Journal of Neuroscience. 1972; 4: 147–166.
66. Sanes D, Rubel E. The ontogeny of inhibition and excitation in the gerbil lateral superior olive. The Journal of Neuroscience. 1988; 8: 682–700.
67. Sanes DH, Goldstein NA, Ostad M, Hillman DE. Dendritic morphology of central auditory neurons correlates with their tonotopic position. The Journal of Comparative Neurology. 1990; 294: 443–454.
68. Rose JE, Greenwood DD, Goldberg JM, Hind JE. Some discharge characteristics of single neurons in the inferior colliculus of the cat. I. Tonotopical organization, relation of spike-counts to tone intensity, and firing patterns of single elements. Journal of Neurophysiology. 1963; 26: 294–320.
69. Merzenich MM, Reid MD. Representation of the cochlea within the inferior colliculus of the cat. Brain Research. 1974; 77: 397–415.
70. FitzPatrick KA. Cellular architecture and topographic organization of the inferior colliculus of the squirrel monkey. The Journal of Comparative Neurology. 1975; 164: 185–207.
71. Stiebler I, Ehret G. Inferior colliculus of the house mouse. I. A quantitative study of tonotopic organization, frequency representation, and tone-threshold distribution. The Journal of Comparative Neurology. 1985; 238: 65–76.
72. Friauf E, Ostwald J. Divergent projections of physiologically characterized rat ventral cochlear nucleus neurons as shown by intra-axonal injection of horseradish peroxidase. Experimental Brain Research. 1988; 73.
73. Sommer I, Lingenhöhl K, Friauf E. Principal cells of the rat medial nucleus of the trapezoid body: an intracellular in vivo study of their physiology and morphology. Experimental Brain Research. 1993; 95: 223–239.

74. Gómez-Álvarez M, Saldaña E. Different tonotopic regions of the lateral superior olive receive a similar combination of afferent inputs. Journal of Comparative Neurology. 2015; 524: 2230–2250.
75. Oliver DL, Beckius GE, Bishop DC, Kuwada S. Simultaneous anterograde labeling of axonal layers from lateral superior olive and dorsal cochlear nucleus in the inferior colliculus of cat. The Journal of Comparative Neurology. 1997; 382: 215-229.
76. Malmierca MS, Saint Marie RL, Merchan MA, Oliver DL. Laminar inputs from dorsal cochlear nucleus and ventral cochlear nucleus to the central nucleus of the inferior colliculus: Two patterns of convergence. Neuroscience. 2005; 136: 883–894.
77. Zheng QY, Johnson KR, Erway LC. Assessment of hearing in 80 inbred strains of mice by ABR threshold analyses. Hearing research. 1999; 130: 94–107.
78. Taberner AM, Liberman MC. Response Properties of Single Auditory Nerve Fibers in the Mouse. Journal of Neurophysiology. 2005; 93: 557–569.
79. Muniak MA, Ayeni FE, Ryugo DK. Hidden hearing loss and endbulbs of Held: Evidence for central pathology before detection of ABR threshold increases. Hearing Research. 2018; 364: 104–117.
80. Paxinos G, Franklin BJ. Paxinos And Franklin's The Mouse Brain In Stereotaxic Coordinates, Compact: The Coronal Plates And Diagrams. 2008.
81. Karnovsky MJ, Roots L. A ‘direct-coloring’ thiocholine method for cholinesterases. Journal of Histochemistry & Cytochemistry. 1964; 12: 219–221.
82. Adobe Photoshop CS. Berkeley, CA: Peachpit Press. In: Bancroft J, Cook H, editors. Manual of histological techniques and their diagnostic application. (1999). Edinburgh: Churchill Livingstone.2021.
83. Brain Map - brain-map.org. 2021. Available online at: https://portal.brain-map.org.
84. Schindelin J, Arganda-Carreras I, Frise E, Kaynig V, Longair M, et al. Fiji: an open-source platform for biological-image analysis. Nature methods. 2012; 9: 676–682.

85. GraphPad Software, I. GraphPad Prism 8. La Jolla, CA. Graphpad.com. 2020. Available online at: <https://www.graphpad.com/guides/prism/7/user-guide/citing_graphpad_prism.htm>
86. Adams JC. Crossed and descending projections to the inferior colliculus. Neuroscience Letters. 1980; 19: 1–5.
87. He Y, Kang SH, Alvarez L. Finding the Skeleton of 2D Shape and Contours: Implementation of Hamilton-Jacobi Skeleton. Image Processing On Line. 2021; 11: 18-36.
88. Scheibel ME, Scheibel AB. Neuropil organization in the superior olive of the cat. Experimental Neurology. 1974; 43: 339–348.
89. Friauf E, Krächan EG, Müller NIC. Lateral Superior Olive. The Oxford Handbook of the Auditory Brainstem.2019; 328–394.
90. Calford MB, Webster WR, Semple MM. Measurement of frequency selectivity of single neurons in the central auditory pathway. Hearing Research. 1983; 11: 395–401.
91. He J. Slow Oscillation in Non-Lemniscal Auditory Thalamus. The Journal of Neuroscience. 2003; 23: 8281–8290.
92. Anderson LA, Linden JF. Physiological differences between histologically defined subdivisions in the mouse auditory thalamus. Hearing Research. 2011; 274: 48–60.
93. Portfors CV, Mayko ZM, Jonson K, Cha GF, Roberts PD. Spatial organization of receptive fields in the auditory midbrain of awake mouse. Neuroscience. 2011; 193: 429–439.
94. Glendenning KK, Brusno-Bechtold JK, Thompson GC, Masterton RB. Ascending auditory afferents to the nuclei of the lateral leminscus. The Journal of Comparative Neurology. 1981; 197: 673–703.
95. Browner RH, Webster DB. Projections of the Trapezoid Body and the Superior Olivary Complex of the Kangaroo Rat (Dipodomys merriami). Brain, Behavior and Evolution. 1975; 11: 338–354.
96. Beyerl BD. Afferent projections to the central nucleus of the inferior colliculus in the rat. Brain Research. 1978; 145: 209–223.

97. Fredrich M, Reisch A, Illing RB. Neuronal subtype identity in the rat auditory brainstem as defined by molecular profile and axonal projection. Experimental Brain Research. 2009; 195: 241–260.
98. Schofield BR, Cant NB. Organization of the superior olivary complex in the guinea pig: II. Patterns of projection from the periolivary nuclei to the inferior colliculus. The Journal of Comparative Neurology. 1992; 317: 438–455.
99. Ramon-Moliner E. An attempt at classifying nerve cells on the basis of their dendritic patterns. The Journal of Comparative Neurology. 1962; 119: 211–227.
100. Morest DK. The neuronal architecture of the medial geniculate body of the cat. Journal of Anatomy. 1962; 98: 611–630.
101. Scheibel ME, Scheibel AB. The organization of the nucleus reticularis thalami: a Golgi study. Brain research. 1966; 1: 43-62.
102. Lu E, Llano DA, Sherman SM. Different distributions of calbindin and calretinin immunostaining across the medial and dorsal divisions of the mouse medial geniculate body. Hearing Research. 2009; 257: 16–23.
103. Lund RD, Webster KE. Thalamic afferents from the spinal cord and trigeminal nuclei. An experimental anatomical study in the rat. The Journal of Comparative Neurology. 1967; 130: 313–327.
104. Malmierca MS, Blackstad TW, Osen KK. Computer-assisted 3-D reconstructions of Golgi-impregnated neurons in the cortical regions of the inferior colliculus of rat. Hearing Research. 2011; 274:13–26.
105. Erickson RP, Hall WC, Jane JA, Snyder M, Diamond IT. Organization of the posterior dorsal thalamus of the hedgehog. The Journal of Comparative Neurology. 1967; 131: 103–130.
106. Wepsic JG. Multimodal sensory activation of cells in the magnocellular medial geniculate nucleus. Experimental Neurology. 1966; 15: 299–318.
107. Aitkin LM. Medial geniculate body of the cat: responses to tonal stimuli of neurons in medial division. Journal of Neurophysiology. 1973; 36: 275–283.

108. Liu M, Dai J, Zhou M, Liu J, Ge X, et al. Mini-review: The neural circuits of the non-lemniscal inferior colliculus. Neuroscience Letters. 2022; 776: 136567.
109. Warr, W Bruce, Beck Boche J, Neely ST. Efferent innervation of the inner hair cell region: origins and terminations of two lateral olivocochlear systems. Hearing Research. 1997; 108: 89–111.
110. Brown MC. Fiber pathways and branching patterns of biocytin-labeled olivocochlear neurons in the mouse brainstem. Journal of comparative neurology. 1993; 337: 600-613.
111. Brown MC. Morphology of labeled afferent fibers in the guinea pig cochlea. The Journal of Comparative Neurology. 1987; 260: 591–604.
112. Hu B. Functional organization of lemniscal and nonlemniscal auditory thalamus. Experimental Brain Research. 2003; 153: 543–549.
113. Komura Y, Tamura R, Uwano T, Nishijo H, Ono T. Transmodal coding for reward prediction in the audiovisual thalamus. International Congress Series. 2003; 1250: 383–396.
114. Suthakar K. Changes in the descending auditory system in hearing loss: focus on auditory efferents. PhD thesis, University of New South Wales, Sydney, New South Wales, AUS. 2016.
115. Rockel AJ, Jones EG. The neuronal organization of the inferior colliculus of the adult cat. I. The central nucleus. Journal of Comparative Neurology. 1973; 147: 11-59.
116. Aitkin LM, Webster WR. Tonotopic organization in the medial geniculate body of the cat. Brain Research. 1971; 26: 402–405.
117. Bourk TR, Mielcarz JP, Norris BE. Tonotopic organization of the anteroventral cochlear nucleus of the cat. Hearing Research. 1981; 4: 215–241.
118. Imig TJ, Morel A. Tonotopic organization in ventral nucleus of medial geniculate body in the cat. Journal of Neurophysiology. 1985; 53: 309–340.
119. Ryugo DK, May SK. The projections of intracellularly labeled auditory nerve fibers to the dorsal cochlear nucleus

of cats. The Journal of Comparative Neurology. 1993; 329: 20–35.
120. Spirou GA, May BJ, Wright DD, Ryugo DK. Frequency organization of the dorsal cochlear nucleus in cats. The Journal of Comparative Neurology. 1993; 329: 36–52.
121. Muniak MA, Rivas A, Montey KL, May BJ, Francis HW, et al. 3D model of frequency representation in the cochlear nucleus of the CBA/J mouse. Journal of Comparative Neurology. 2013; 521: 1510–1532.
122. Ramón y Cajal S. Histologie du Systeme Nerveux de L'Homme et des Vertebres, 1. Paris: Maloine. 1909.
123. Henkel CK, Brunso-Bechtold JK. Calcium-binding proteins and GABA reveal spatial segregation of cell types within the developing lateral superior olivary nucleus of the ferret. Microscopy Research and Technique. 1998; 41: 234–245.
124. Kulesza RJ. Cytoarchitecture of the human superior olivary complex: Medial and lateral superior olive. Hear. Res. 2007; 225: 80–90.
125. Brown MC, Levine JL. Dendrites of medial olivocochlear neurons in mouse. Neuroscience. 2008; 154: 147–159.
126. Liberman MC, Brown MC. Physiology and anatomy of single olivocochlear neurons in the cat. Hearing Research. 1986; 24: 17–36.
127. Tsuchitani C. Functional organization of lateral cell groups of cat superior olivary complex. Journal of Neurophysiology. 1977; 40: 296–318.
128. Tollin DJ, Yin TCT. The Coding of Spatial Location by Single Units in the Lateral Superior Olive of the Cat. II. The Determinants of Spatial Receptive Fields in Azimuth. The Journal of Neuroscience. 2002; 22: 1468–1479.
129. Vetter DE, Adams JC, Mugnaini E. Chemically distinct rat olivocochlear neurons. Synapse. 1991; 7: 21–43.
130. Kandler K, Kullmann P, Ene F, Kim G. Excitatory action of an immature glycinergic/GABAergic sound localization pathway. Physiology & Behavior. 2002; 77: 583–587.
131. Maison SF, Adams JC, Liberman MC. Olivocochlear innervation in the mouse: Immunocytochemical maps, crossed versus uncrossed contributions, and transmitter

colocalization. The Journal of Comparative Neurology. 2002; 455: 406–416.
132. Nabekura J, Katsurabayashi S, Kakazu Y, Shibata S, Matsubara A, et al. Developmental switch from GABA to glycine release in single central synaptic terminals. Nature Neuroscience. 2003; 7: 17–23.
133. Niu X, Bogdanovic N, Canlon B. The distribution and the modulation of tyrosine hydroxylase immunoreactivity in the lateral olivocochlear system of the guinea-pig. Neuroscience. 2004; 125: 725–733.
134. Wu JS, Yi E, Manca M, Javaid H, Lauer AM, et al. Sound exposure dynamically induces dopamine synthesis in cholinergic LOC efferents for feedback to auditory nerve fibers. eLife. 2020; 19.
135. Glendenning KK, Baker BN, Hutson KA, Masterton RB. Acoustic chiasm V: Inhibition and excitation in the ipsilateral and contralateral projections of LSO. The Journal of Comparative Neurology. 1992; 319: 100–122.
136. Finlayson PG, Caspary DM. Low-frequency neurons in the lateral superior olive exhibit phase-sensitive binaural inhibition. Journal of Neurophysiology. 1991; 65: 598–605.
137. Brunso-Bechtold JK, Linville MC, Henkel CK. Terminal types on ipsilaterally and contralaterally projecting lateral superior olive cells. Hearing Research. 1994; 77: 99–104.
138. Fisher M, Llewellyn G. The Mongolian gerbil: natural history, care, and maintenance.. American Biology Teacher. 1978; 40: 557-560.
139. Okanoya K, Yosida S, Barone CM, Applegate DT, Brittan-Powell EF, et al. Auditory-vocal coupling in the naked mole-rat, a mammal with poor auditory thresholds. Journal of Comparative Physiology A. 2018; 204: 905–914.
140. Heth G, Frankenberg E, Nevo E. Adaptive optimal sound for vocal communication in tunnels of a subterranean mammal (Spalax ehrenbergi). Experientia. 1986; 42: 1287–1289.
141. Barker AJ, Koch Lewin GR, Pyott SJ. Hearing and vocalizations in the naked mole-rat. Advances in Experimental Medicine and Biology. 2021; 1319: 157-195.
142. Merzenich MM, Kitzes L, Aitkin L. Anatomical and physiological evidence for auditory specialization in the

mountain beaver (aplodontia rufa). Brain Research. 1973; 58: 331–344.

143. Heffner RS, Heffner HE. Degenerate hearing and sound localization in naked mole rats (Heterocephalus glaber), with an overview of central auditory structures. The Journal of Comparative Neurology. 1993; 331: 418–433.

144. Ehret G, Riecke S. Mice and humans perceive multiharmonic communication sounds in the same way. Proceedings of the National Academy of Sciences. 2001; 99: 479–482.

145. Portfors CV, Perkel DJ. The role of ultrasonic vocalizations in mouse communication. Current Opinion in Neurobiology. 2014; 28: 115–120.

Supplementary Materials

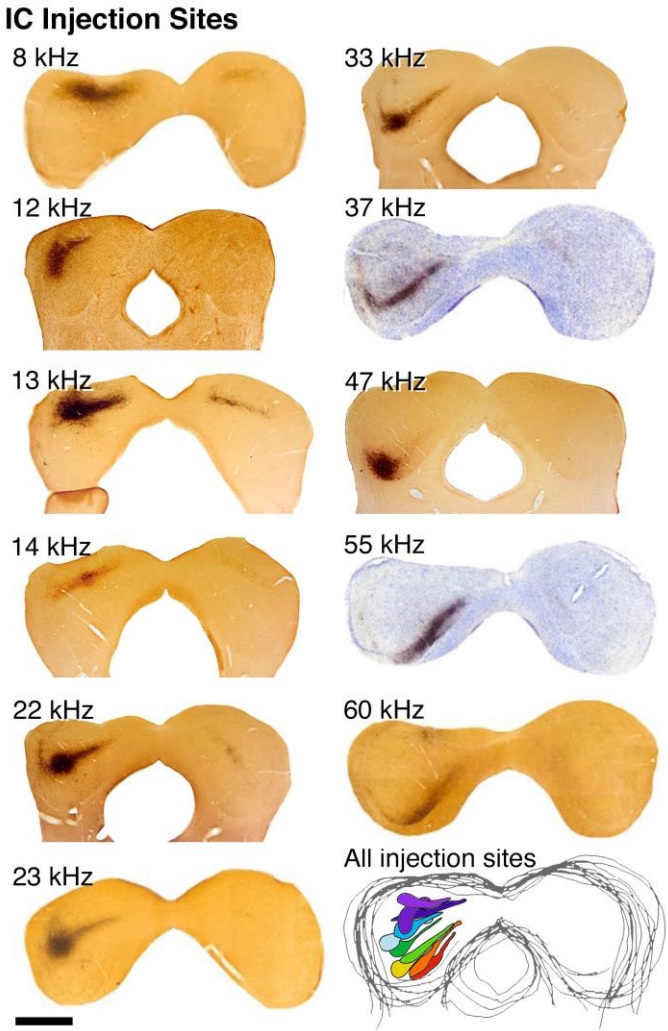

Supplementary Figure 1: Photomicrographs through the middle of the injection sites in coronal sections of the mouse IC. When reconstructed in 3D, each injection site formed a layer approximately 50-100 µm thick. These are combined in the drawing at the bottom right illustrating the tonotopic organization. *Abbreviations:* inferior colliculus (IC); kilohertz (kHz). Scale bar = 250 µm.

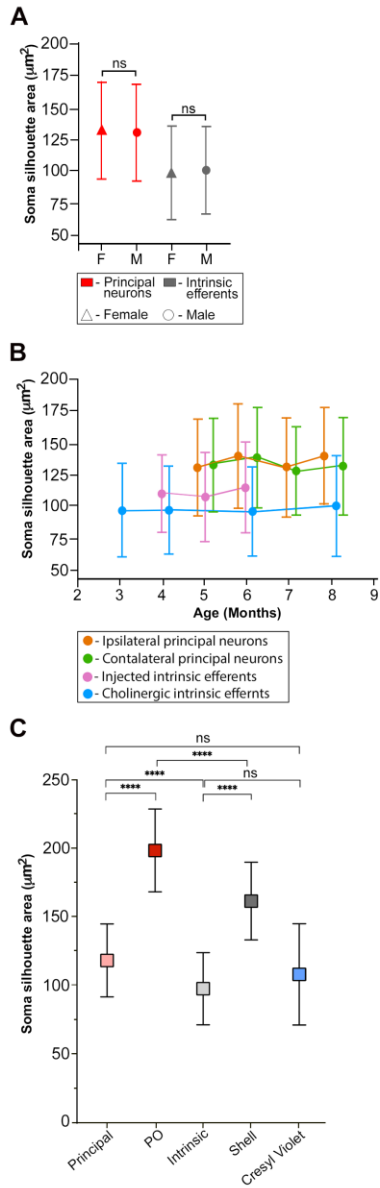

Supplementary Figure 2: Plots of cell body sizes for major neurons of the LSO in male and female mice.

A. The mean and standard deviation for the cell body silhouette area was calculated for principal and intrinsic neurons and for male and female mice. Overall, there is no difference in principal (*p=0.9998*) or intrinsic (*p=0.9707*)

cell body size between the sexes. **B.** Likewise, there are no size changes with respect to age (from 3-8 months). **C.** The data represent four classes identified by their projections and cell body location: Principal, PO, intrinsic and shell neurons. A two-way ANOVA revealed significant differences between the principal, PO, intrinsic, and shell neurons. As expected, there are no size differences between the CV labeled neurons and the principal neurons ($F(105,438) = 0.86$, $p=0.8408$) or the CV labeled neurons and the intrinsic efferents ($F(1,103) = 3.09$, $p=0.0816$). *Abbreviations:* Female (F); male (M); periolivary (PO).

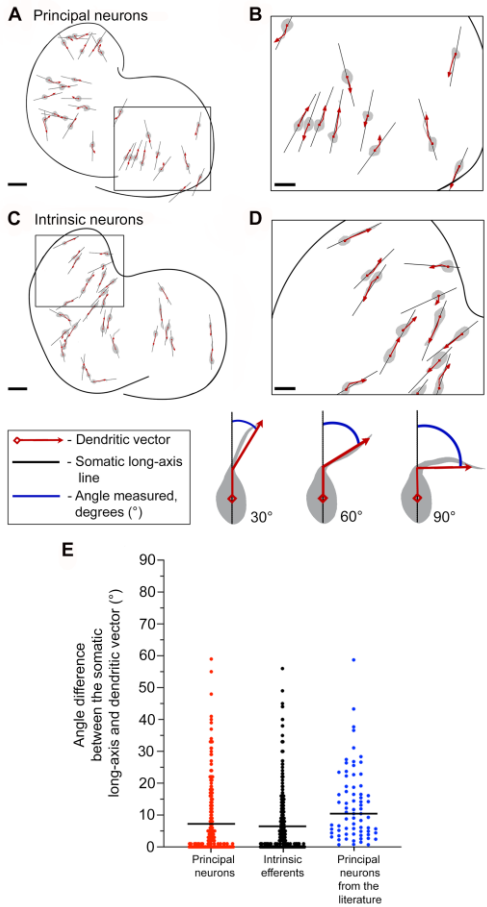

Supplementary Figure 3: Soma long axis and dendritic vector analysis in the LSO revealed no significant difference when comparing angle orientation of the two neuronal features.

A. Drawing illustrates alignment of somatic long axis (black line) and dendritic vectors (red arrow) of principal neurons (gray) in a middle LSO section. **B.** A higher magnification of the ventromedial area outlined in A,

illustrating the frequent alignment of soma and dendrites. **C.** Drawing of somatic long axis and dendritic vectors of intrinsic efferent neurons in the middle LSO section. **D.** A higher magnification of the boxed area in C, showing frequent alignment between soma and dendrites. *Key*: Angles of 30°, 60° and 90° degrees are included for reference. Note the general alignment between cell orientation and its dendritic vector. Scale bar equals 100 µm (A, C) and 50 µm (B, D). **E.** Plot of the angle (˚) differences between soma long axes and dendritic vectors of labeled principal and intrinsic efferent neurons. The angles between the long axis and dendrite vector of each individual principal (red), intrinsic efferent (black) and Golgi and intracellularly labeled principal neurons from the literature (blue) were calculated. The points on the plot represent the angle difference for each neuron analysed. Golgi and intracellular labeling of principal neurons from the literature of cat, gerbil, mouse, rat and human LSO principal cells were included. These data illustrate that somatic orientation infers the overall dendritic orientation.

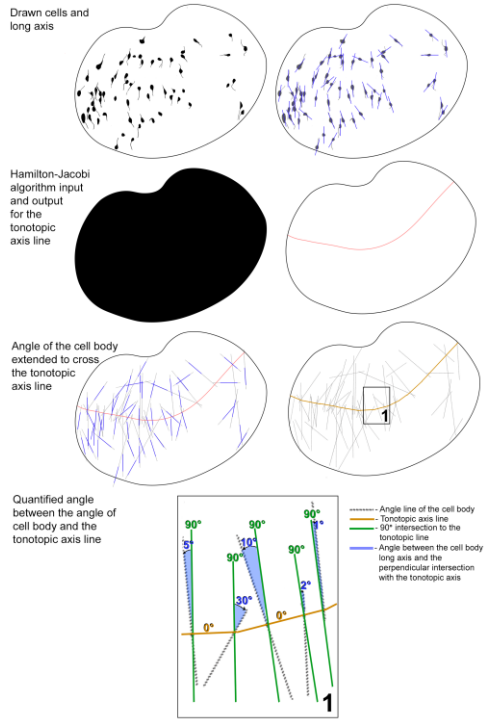

Supplementary Figure 4: Method process for quantifying neuronal alignment with the tonotopic axis.
A series of LSO sections with labeled LSO neurons from an IC injections, cochlear injections, or cholinergic staining were traced, analysed for somatic orientation and quantified against a tonotopic axis derived from the Hamilton Jacobi algorithm. A single representative section is shown. The first steps for

this analysis was to trace the LSO border and labeled cells (top row, left). The traced neurons were put through a FIJI script to show the output of the somatic long axis for each cell represented by a blue line (top row, right). The shape of the LSO nucleus was processed as a binary image (second row, left) into the Hamilton Jacobi algorithm to produce a skeletal output of the LSO nucleus shape to represent a tonotopic axis (red line, second row, right). The FIJI output of the somatic long-axes lines (blue) was superimposed onto the red tonotopic axis line derived from the algorithm (third row, left). A grey dashed line was extended from the blue somatic long axis line to intersect with the tonotopic axis so the angles could be readily calculated as seen in the inset region (third row, right). Inset region: examples for how the angle (blue) for each somatic long axis line (grey) was calculated against the perpendicular intersection at that point along the tonotopic axis (green, 90 degrees) and converted as an absolute value. A smaller angle difference inferred that the cell was orientation perpendicular to the tonotopic axis.

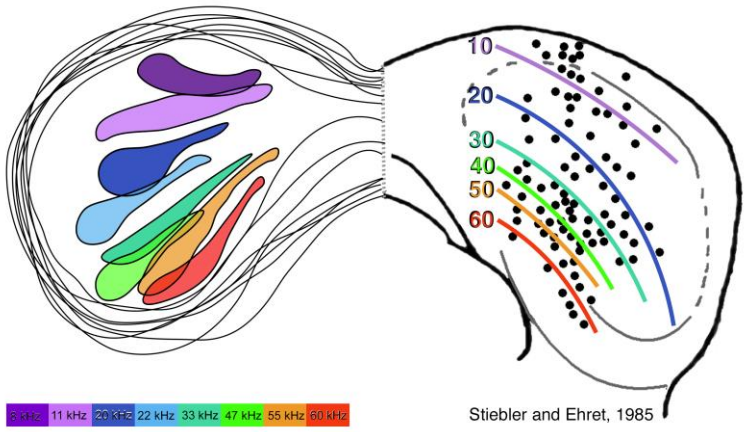

Supplementary Material 5: Comparison of anatomically derived isofrequency layers (left) and electrophysiologically derived isofrequency lines (right). The anatomical laminae represent a collection of reconstructed profiles of chromogenically-recovered injection sites at their midpoint from CBA/CaH mice. Profiles are color coded with respect to the frequency spectrum (lower left). The isofrequency lines were taken from Figure 7B (Stiebler and Ehret, 1985) where they connected points of equivalent frequency as recorded in the IC of the house mouse. We color coded their map to the frequency spectrum. The tonotopic organization for the IC is remarkably consistent given the different methods, histology, mouse strains, and eras. *Abbreviation:* kilohertz (kHz).

Supplementary Table 1: Cell body silhouette area (μm^2) showing the similarity in principal and intrinsic cell size for mice aged between 3-8 months. Two-way ANOVA testing revealed no significant difference in cell size for neurons labeled in mice aged 3-8 months old for all cell types: ipsilateral and contralateral principal neurons, cholinergic neurons, and injected neurons ($F(1318, 1287) = 0.99$, $p=0.5728$).

	Principal Neurons		**Intrinsic Neurons**	
	Ipsilateral	Contralateral	Cholinergic	Injected
Number of cases	4	4	7	5
Ages (months)	6, 7, 8	6, 7, 8	3, 4, 6, 8	4, 5, 6
Number of cells	679	611	1121	647
Median area (μm^2)	124.4	126.5	84.67	106.8
Mean (μm^2) ± St. Dev	129.3 ± 37.37	131.2 ± 36.87	97.92 ± 36.40	109.4 ± 33.78

Supplementary Table 2: Cell body silhouette area (μm^2) showing the similarity in principal and intrinsic cell size for male and female mice. Two-way ANOVA testing revealed no significant difference in cell size between principal neurons labeled in female and male mice ($F(1,713) = 0.09$, $p=0.7702$) and between intrinsic neurons labeled in either sex ($F(1,443) = 0.67$, $p=0.4127$).

	Female		**Male**	
Neurons:	Principal	Intrinsic	Principal	Intrinsic
Number of cases	5	5	5	5
Number of cells	915	745	1170	802
Median area (μm^2)	123.4	88.41	126.7	96.79
Mean (μm^2) ± St. Dev	126.5 ± 37.41	100.7 ± 36.40	128.0 ± 37.19	103.1 ± 33.69

Supplementary Table 3: Cell body silhouette area (µm2) for the LSO neuronal cohorts stained by different methods. A T-test revealed no statistically significant difference exists between the ipsilateral and contralateral principal LSO neurons (*p=0.4126*). Two-way ANOVA testing compared the three methods of labeling the intrinsic neurons and revealed no significant difference ($F(61,84) = 0.59$, *p=0.9845*).

	Principal Neurons		**Intrinsic Neurons**		
	Ipsilateral	Contralateral	ChAT	AChE	Injected
Number of cases	4	4	4	3	5
Number of cells	679	611	369	243	430
Median (μm^2)	124.4	126.5	83.77	84.75	107.1
Mean (μm^2) ± St. Dev	129.3 ± 37.37	131.2 ± 36.87	94.02 ± 33.44	96.23 ± 38.22	110.9 ± 33.38

Supplementary Table 4: Angle measurements between cell body long axis and corresponding dendritic vector of labeled LSO principal and intrinsic neurons. Small degree values indicate close alignment between cell body long axis and dendritic vectors.

	Principal	Intrinsic
Number of cases	3	3
Number of cells	298	384
Median (degrees°)	3.00	3.00
Mean ± SD (degrees°)	7.24 ± 10.42	6.49 ± 9.33

Supplementary Table 5: Descriptive statistics of LSO neuron subclasses and their alignment to the perpendicular intersection with the tonotopic axis. Principal and intrinsic neurons have greater alignment to the perpendicular intersection with the tonotopic axis than the periolivary and shell neurons. Angle deviations below 45 degrees indicate parallel alignment to the perpendicular intersection, and angle deviations above 45 degrees indicate perpendicularity. *Abbreviations*: Principal neurons (P); Periolivary neurons (PO); Intrinsic neurons (I); Shell neurons (S). Regardless of the position in the LSO, the principal and intrinsic neurons are aligned: Rostral – *p=0.0824*; Middle – *p=0.0694*; Caudal – *p=0.1643*; Total – *p=0.0612*.

	Rostral				**Middle**				**Caudal**			
	P	PO	I	S	P	PO	I	S	P	PO	I	S
Number of cases	5	5	5	5	5	5	5	5	5	5	5	5
Number of cells	121	11	113	7	367	29	379	21	181	23	170	19
Median (degrees°)	43.00	68.00	33.00	71.00	25.00	73.00	23.00	71.00	30.00	73.00	30.00	74.00
Mean ± SD (degrees°)	40.25 ± 23.58	64.18 ± 17.90	35.10 ± 24.98	64.14 ± 13.04	30.56 ± 25.04	61.28 ± 24.62	27.95 ± 22.10	59.71 ± 24.39	33.06 ± 23.31	68.22 ± 16.26	30.03 ± 21.20	67.32 ± 20.16